Multi-Walled Carbon Nanotube Filter for Detaining Immunosuppressive T-Cells and Inducing the Activation of Effector T-Cells

Gemma Di Placido

Master's Thesis

Department of Chemical Engineering

McGill University, Montreal, Quebec

December 2024

Supervised by

Prof. Sylvain Coulombe, McGill University

Prof. Philip Wong, University of Toronto

A thesis submitted to McGill University in partial fulfillment of the requirements of the degree of Master of Science in Chemical Engineering

Abstract

Cancer is a major public health concern worldwide and the main cause of death in Canada. It remains challenging to effectively treat cancer given its ability to evade and suppress immune responses. Adoptive T-cell transfer (ACT) has recently gained popularity as a promising cancer immunotherapy. ACT works on the premise of enhancing the effectiveness of autologous white blood cells. T-cells are a type of white blood cell that play a critical role in killing cancer cells. However, regulatory T (T_{reg}) cells are immunosuppressive and prevent the cancer-killing effector T (T_{eff}) cells from eliminating cancer cells. A plasma functionalized multi-walled carbon nanotube (MWCNT) filter was developed with future intentions of detaining T_{reg} cells and activating T_{eff} cells using mechanical forces and non-biological agonists. MWCNTs are a network of cylindrically rolled carbon atoms used as the base of the filter material given its attractive material properties. The MWCNT coating was made functional to biological systems by modifying its surface using an ammonia plasma treatment, namely plasma-enhanced chemical vapor deposition. Amine (NH_2) functional groups were grafted onto the surface of the MWCNTs which allow for future immobilization of target antibodies. The surfaces of the MWCNT and NH_2-MWCNT filters were analyzed by scanning electron microscopy, X-ray photoelectron spectroscopy, water contact angle goniometry, and Raman spectroscopy. High purity superhydrophobic MWCNT filters were synthesized by chemical vapor deposition and contained a carbon content of 98.9 %. The surfaces of NH_2-MWCNT filters became hydrophilic after ammonia functionalization. The D band and G band intensity ratios of the MWCNT and NH_2-MWCNTfilters were 0.45 and 0.53, respectively, which confirmed the presence of NH_2 functional groups on the surface of the MWCNTs. A splenocyte suspension was normally dispensed through the MWCNT and NH_2-MWCNT filters. Spleen cell viability experiments were performed using fluorescence microscopy. Probability (p)-

values of 0.44 and 0.16 were computed for the spleen cell viability experiments through the MWCNT and NH_2-MWCNT filters, respectively. The high p-values suggested that the interaction of the splenocytes with the MWCNT and NH_2-MWCNT filters were not statistically significant in influencing the viability of the cells. Mouse interferon (IFN)-γ ELISA assays were performed to measure the quantity of cytokines released in the filtered splenocyte suspension after applied normal stresses through the MWCNT and NH_2-MWCNT filters. Low quantities of less than 3 pg/mL of IFN-γ were reported in the supernatant of the filtered suspensions. Mechanical forces alone did not induce the activation of T-cells while passing through the filters. The combination of mechanically dispensing T-cells through NH_2-MWCNT filters coated with immobilized target antibodies may lead to the selective enhancement and proliferation of T-cells.

Résumé

Le cancer est un problème de santé publique mondiale et la principale cause de décès au Canada. Il reste difficile de traiter efficacement le cancer en raison de sa capacité à échapper aux réponses immunitaires et à les supprimer. Le transfert adoptif de cellules T (ACT) a récemment gagné en popularité en tant qu'immunothérapie prometteuse contre le cancer. L'ACT repose sur le principe de l'amélioration de l'efficacité des globules blancs autologues. Les lymphocytes T sont un type de globules blancs qui jouent un rôle essentiel dans la destruction des cellules cancéreuses. Cependant, les cellules T régulatrices (T_{reg}) sont immunosuppressives et empêchent les cellules T effectrices (T_{eff}) d'éliminer les cellules cancéreuses. Un filtre MWCNT fonctionnalisé au plasma a été mis au point dans le but de retenir les cellules T_{reg} et d'activer les cellules T_{eff} à l'aide de forces mécaniques et d'agonistes non biologiques. Les nanotubes de carbone multiparois (MWCNT) sont un réseau d'atomes de carbone enroulés cylindriquement, utilisé comme base du matériau filtrant en raison de ses propriétés matérielles attrayantes. Le revêtement de MWCNT a été rendu fonctionnel pour les systèmes biologiques en modifiant sa surface à l'aide d'un traitement au plasma d'ammoniac, à savoir le dépôt chimique en phase vapeur assisté par plasma. Des groupes fonctionnels amine (NH_2) ont été greffés sur la surface des MWCNT, ce qui permet l'immobilisation future d'anticorps cibles. Les surfaces des filtres MWCNT et NH_2-MWCNT ont été analysées par microscopie électronique à balayage, spectroscopie photoélectronique à rayons X, goniométrie de l'angle de contact avec l'eau et spectroscopie Raman. Des filtres MWCNT superhydrophobes de grande pureté ont été synthétisés par dépôt chimique en phase vapeur et contenaient 98.9 % de carbone. Les surfaces des filtres NH_2-MWCNT sont devenues hydrophiles après fonctionnalisation à l'ammoniac. Les rapports d'intensité de la bande D et de la bande G des filtres MWCNT et NH_2-MWCNT étaient respectivement de 0.45 et 0.55, ce qui confirme la

présence de groupes fonctionnels NH_2 à la surface des MWCNT. Une suspension de splénocytes a été normalement distribuée à travers les filtres MWCNT et NH_2-MWCNT. Des expériences sur la viabilité des cellules de la rate ont été réalisées à l'aide de la microscopie à fluorescence. Des valeurs de probabilité (p) de 0.44 et 0.16 ont été calculées pour les expériences de viabilité des cellules de la rate à travers les filtres MWCNT et NH_2-MWCNT, respectivement. Les valeurs p élevées suggèrent que l'interaction des splénocytes avec les filtres MWCNT et NH_2-MWCNT n'était pas statistiquement significative pour influencer la viabilité des cellules. Des tests ELISA de l'interféron (IFN)-γ de souris ont été réalisés pour mesurer la quantité de cytokines libérées dans la suspension de splénocytes filtrée après l'application de contraintes normales à travers les filtres MWCNT et NH_2-MWCNT. De faibles quantités d'IFN-γ, inférieures à 3 pg/mL, ont été rapportées dans le surnageant des suspensions filtrées. Les forces mécaniques seules n'ont pas induit l'activation des cellules T lors de leur passage à travers les filtres. La combinaison de la distribution mécanique de cellules T à travers des filtres NH_2-MWCNT recouverts d'anticorps cibles immobilisés peut conduire à l'augmentation sélective et à la prolifération des cellules T.

Acknowledgments

It is my pleasure to acknowledge the following people who collectively have contributed to the completion of my Master's degree.

Thank you to my primary supervisor, Sylvain Coulombe for allowing me to join the CPPE laboratory. You have managed to foster a harmonious environment that encourages us to help one another. It is an honour to be part of your team and I am fortunate to advance into my doctoral studies under your supervision. You have guided and helped shape me into the young researcher that I am today. I sincerely thank you for your patience and compassion.

Thank you, Philip Wong, for welcoming me into your laboratory at the University of Montreal Hospital Research Centre (CR-CHUM). Your enthusiasm and passion towards advancing in your research is inspirational. Your team of researchers are kind, skilled, and knowledgeable. My transition to the CR-CHUM has been facilitated by Audrey Glory, Elena-Refet Mollof, Julie Lafontaine, Maryam Ziaee, and Rodin Chermat. Thank you all for your patience in introducing me to your equipment, machinery and practices.

Thank you to the members of the CPPE team. Lynn Hein, you introduced me to your project during my first year in the CPPE laboratory which inspired me to pursue research in a similar field. I was fortunate to have had the opportunity to be mentored by an organized and proficient researcher like you. Thank you, Dante Filice, Philip Cimento and Steven Walker, for being friendly in the corridors and assisting me whenever needed.

Thank you to the technical staff at McGill University in the Chemical Engineering department. Thank you, Andrew Golsztajn, for training me on the equipment in the analytical laboratory. You were always available to answer any technical questions I had.

A sincere thank you to my family and friends for supporting me throughout my journey as a graduate student. Thank you to my parents, sister and boyfriend. My parents have provided me with an ample amount of opportunities and unconditional love. I am forever thankful to you, mom and dad.

Table of Contents

List of Figures

List of Tables

List of Abbreviations

Abbreviation	Description
ACT	Adoptive cell transfer
Ab	Antibody
mAb	Monoclonal antibody
Ag	Antigen
APC	Antigen-presenting cell
CAA	Cancer associated antigens
CAR	Chimeric antigen receptor
CD3	Cluster of differentiation 3
CIPA	Comité institutional de protection des animaux
CR-CHUM	The University of Montreal Hospital Research Center
CNT	Carbon nanotube
CPPE	Catalytic & Plasma Process Engineering
ELISA	Enzyme-linked immunosorbent assay
Fab	Fragment antigen binding
Fc	Fragment crystallisable
FOV	Field of view
GFP	Green fluorescent protein
Ig	Immunoglobulin
IFN	Interferon
IL-2	Interleukin 2
MHC	Major histocompatibility complex
pMHC	Peptide major histocompatibility complex

MWCNT	Multi-walled carbon nanotube
NH_2-MWCNT	Amine-covered multi-walled carbon nanotubes
OCA	Optical contact angle
RBC	Red blood cell
SEM	Scanning electron microscopy
SWCNT	Single-walled carbon nanotube
SS	Stainless steel
SOP	Standard operating procedure
PECVD	Plasma-enhanced chemical vapor deposition
t-CVD	Thermal chemical vapor deposition
TCR	T-cell receptor
TIL	Tumour infiltrating lymphocytes
TL	Transmitted light
T_{eff}	Effector T-cells
T_m	Memory T-cells
T_{reg}	Regulatory T-cells
UV	Ultraviolet
WBC	White blood cell
WCA	Water contact angle
XPS	X-ray photoelectron spectroscopy

Chapter 1

1. Introduction

Substantial effort has been devoted to cancer treatment. Despite this, cancer remains the main cause of death in Canada as every two out of five people are expected to be diagnosed in their lifetime [1]. Conventional therapies such as radiotherapy and chemotherapy are not always effective as cancer exhibits heterogeneity, genetic mutability and immunosuppression [2]. Recently, a promising immunotherapy technique has immerged, namely adoptive cell transfer (ACT). ACT enhances the effectiveness and functionalities of a patient's own immune cells through *ex vivo* genetic and cellular engineering practices [3].

The immune system is the body's natural defence against bacteria, viruses, toxins, allergens and abnormal cells such as cancer. The adaptive immune system is a type of immune system that is divided into cell-mediated immunity and humoral-immunity elicited by T-lymphocytes (T-cells) and B-lymphocytes (B-cells), respectively. Upon activation of T-cells, cell-mediated immune responses occur in which T-cells proliferate and differentiate into effector T (T_{eff}) cells and memory T (T_m) cells. T_{eff} cells contribute to the identification and elimination of foreign substances [4]. Immunosuppressive cells, regulatory T (T_{reg}) cells also compromise the efficacy of T_{eff} cells by hindering immune responses [5].

Therefore, the aim of this project is to enhance the efficacy of ACT technology by offering a two-in-one *ex vivo* filtration strategy. A functional nanomaterial filter will be developed that selectively detains immunosuppressive T-cells and induces the activation of T_{eff} cells by mechanical forces and non-physiological agonists. The filter material will be composed of a network of multi-walled carbon nanotubes (MWCNTs) synthesized on a metallic surface, specifically, a stainless steel (SS)

mesh. The MWCNT filter will be plasma processed as to modify the surface and render it functional for the potential binding of biological agents. Immunosuppressive T-cells will be detained by immobilizing target antibodies (Abs) onto the plasma-functionalized MWCNT filter. Non-physiological agonists such as anti-CD3 monoclonal antibodies (anti-CD3 mAbs) will also be attached to the filter which will identify, isolate and induce the activation of T_{eff} cells. The activation of T_{eff} cells will trigger the cascade of events leading to cancer cell death.

Chapter 2

2. Literature review

2.1. Filter material

2.1.1. MWCNT filters

2.1.1.1. MWCNT

Carbon is ubiquitous in nature and forms many different allotropes. A carbon nanotube (CNT) is a cylindrically rolled sheet of sp^2-hybridized carbons atoms arranged in a hexagonal configuration (graphene) [6]. CNTs are differentiated by their number of concentric graphene cylinders being either single-walled carbon nanotubes (SWCNTs) or MWCNTs, as displayed in Figure 1 [7].

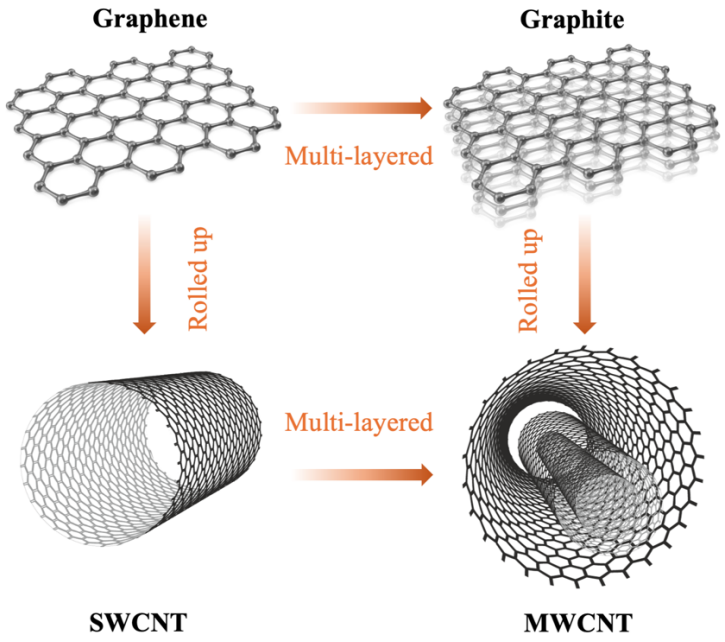

Figure 1: Different allotropes of carbon

CNTs are emerging in popularity as a base nanomaterial for potential biomedical applications [8]. The gained traction is attributed to their attractive material properties, including thermal and electrical conductivity [7]. MWCNTs show exceptional mechanical performance and structural integrity due to their rolled graphitic structure [6]. Other valuable properties include their high surface area and aspect ratio. Hence, a filter made of this carbon nanostructure would allow for greater stresses of fluid to be applied over larger areas of liquid-cell interactions.

2.1.1.2. MWCNT synthesis

Thermal chemical vapor deposition (t-CVD) is a widely accepted thin-film deposition technique that is used to synthesize a homogenous coating of MWCNTs on metallic surfaces. For successful synthesis of MWCNTs by t-CVD, a precursor gas must interact with a catalyst on a substrate while being exposed to elevated temperatures. Common transition metals used as the catalyst nanoparticle include iron (Fe), cobalt (Co), nickel (Ni), and molybdenum (Mo) [9]. The flow of a hydrocarbon gas provides the source of carbon to be deposited onto the substrate. Typical hydrocarbon gases are acetylene (C_2H_2), ethylene (C_2H_4), and methane (CH_4). The t-CVD process involves a series of actions that must be effected sequentially at elevated temperatures (600˚C – 1000˚C) [10]. The order is displayed in Figure 2 specific to MWCNT growth on a 316L SS surface.

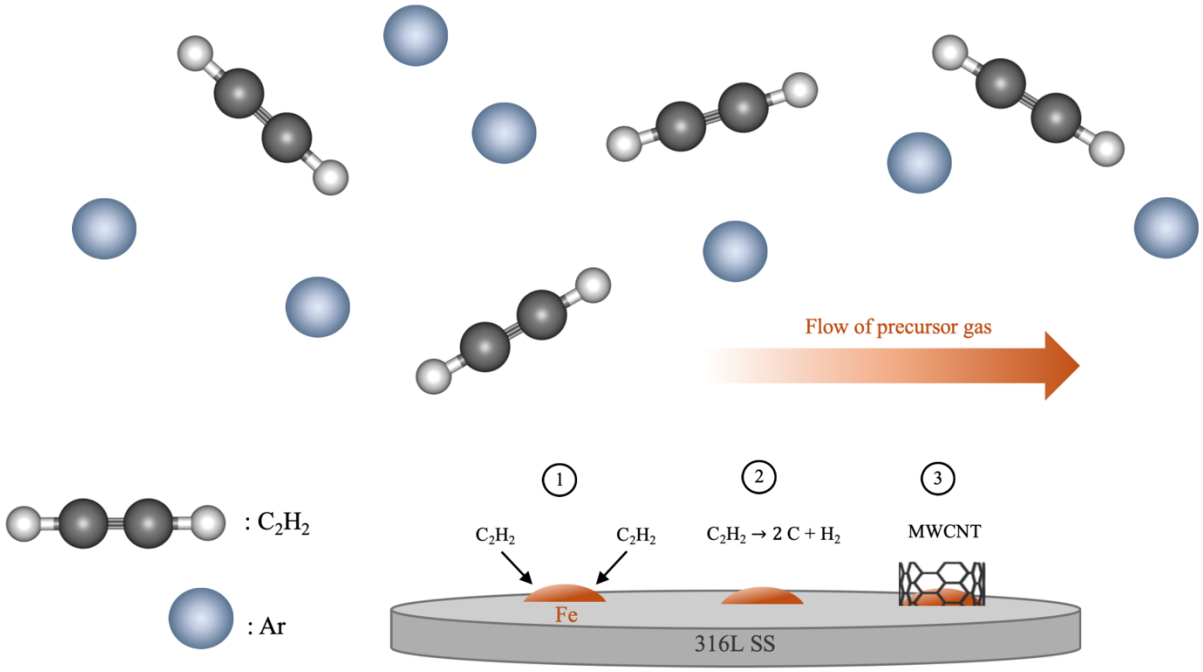

Figure 2: MWCNT synthesis steps: (1) Adsorption of C_2H_2 onto surface (2) Surface decomposition of C_2H_2 (3) Nucleation of MWCNTs

(1) Adsorption of C_2H_2 onto surface: The hydrocarbon precursor (C_2H_2) binds to the catalyst nanoparticle (Fe) on the surface of the SS substrate.

(2) Surface decomposition of C_2H_2: C_2H_2 decomposes at the surface into its constituent carbon and hydrogen atoms.

(3) Nucleation of MWCNTs: The carbon dissolves into the Fe until saturation. After which, the carbon begins to precipitate out and initiate surface nucleation of MWCNTs [11].

Other employed methods of synthesis are laser ablation and arc-discharge [10]. CVD poses advantages over the other methods for lab-scale experiments by requiring significantly lower temperatures by threefold. CVD allows for a high yield of CNTs with control over their morphology (size and shape), structure (SWCNTs or MWCNTs) and alignment (growth direction) [9].

2.1.2. NH_2-MWCNT filters

2.1.2.1. NH_2-MWCNT

Despite their appealing characteristics, MWCNTs are hydrophobic in nature which limits their use in chemical and biological systems [12, 13]. Modifying the surface of the MWCNT filters is required to enhance the surface characteristics and render the filters biocompatible. By broadening their range of applicability in physiological systems, biological agents can be bound onto the surface of the modified MWCNT filters.

Amine functional groups are classified as primary ($R\text{-}NH_2$), secondary ($R_2\text{-}NH$) and tertiary ($R_3\text{-}N$) amines depending on the number of hydrogen atoms bound to the nitrogen atom [14]. Biological molecules like amino acids contain amino groups ($\text{-}NH_2$) that are involved in many physiological processes in the body. Amine-functionalized surfaces, specifically primary amines have a greater affinity to biological molecules such as Abs and support their immobilization on the MWCNT filter [13].

2.1.2.2. Plasma-enhanced chemical vapor deposition

Physical and chemical treatments can be applied to modify the surfaces of materials [15, 16]. Plasma functionalization is a widely accepted physical surface treatment that presents many advantages over wet-chemical methods. Some examples include the avoidance of hazardous chemical solvents, surface contamination and influence on the bulk properties of the material [17]. Hence, functionalizing the surfaces of MWCNTs using plasma treatment avoids MWCNT damage and agglomeration [18].

Plasma-enhanced chemical vapor deposition (PECVD) uses plasma to graft desired functional groups on a variety of material surfaces [19]. Specifically, the PECVD technique using ammonia

(NH_3) as the source of reactive species can be used to anchor NH_2 groups to the surface of the MWCNT filters. The NH_3 plasma constituents are neutral and energized species including radicals, ions and electrons as displayed in Figure 3.

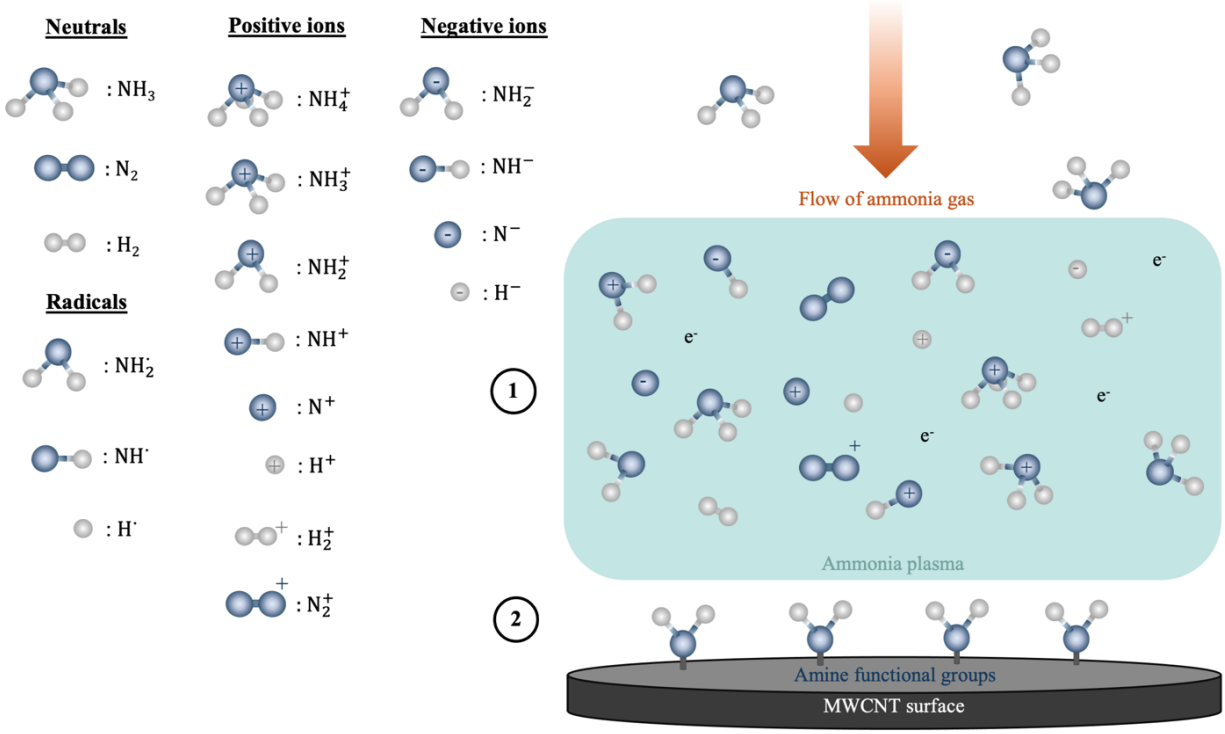

Figure 3: Plasma functionalization (1) Ammonia plasma constituents (2) Amine functional groups grafted on MWCNT surface

The plasma species along with the ultraviolet (UV) light emitted by the plasma, interact with the MWCNT surface and contribute to the breaking of sp^2-hybridized carbons atoms within the MWCNT structure. The breaking of bonds creates active sp^3-hybridized binding sites for reactive species [12].

2.2. Immune responses

2.2.1. Immune cells

Lymphocytes are part of the adaptive immune system that provide specific immune responses to a variety of foreign substances [20]. Typical sizes of murine and human lymphocytes measure 10-15 μm and 9-18 μm in diameter, respectively [21, 22].

2.2.1.1. B-lymphocytes

B-lymphocytes participate in humoral-mediated immunity by producing Abs that circulate within the blood [23]. They also have membrane-bound protein complexes, B-cell receptors (BCR) on their surfaces with variable portions that recognize the same antigen (Ag) as the Abs that the individual cell produce. Both Abs and BCR are generated through genetic recombination during the maturation of B-cells. This process results in an extensive repertoire of Abs and BCRs that can recognize unique Ags [23].

2.2.1.2. T-lymphocytes

T-lymphocytes participate in cell-mediated immunity by recognizing and eliminating cancerous cells or cells infiltrated by pathogens. Similar to B-cells, genes are rearranged in T-cells and give rise to a wide repertoire of T-cell receptors (TCRs) [23]. Despite the abundance of T-cells, only a select few possess the appropriate TCR that can recognize a specific cancer. Therefore, the challenge remains of identifying and isolating cancer-specific T-cells to then clone and activate for the effective destruction of the cancer.

2.2.2. T-cell activation

2.2.2.1. Antigen-specific approach

T-lymphocytes contribute to cell-mediated immune responses which include defence against cancerous cells [24]. T-cell mediated cancer cell death following an Ag-specific approach involves a series of three steps. Firstly, antigen-presenting cells (APCs) interact with cancer cells to acquire their Ags. The cancer associated antigens (CAAs) are presented on the surface of the major histocompatibility complex (MHC) I or II of APCs (pMHC). Secondly, T-cell activation occurs in which naïve CD_4^+ T_h cells and CD_8^+ T_c cells become T_{eff} cells. All T-cells express transmembrane proteins consisting of a TCR and a cluster of differentiation 3 (CD3) as displayed by Figure 4 [25].

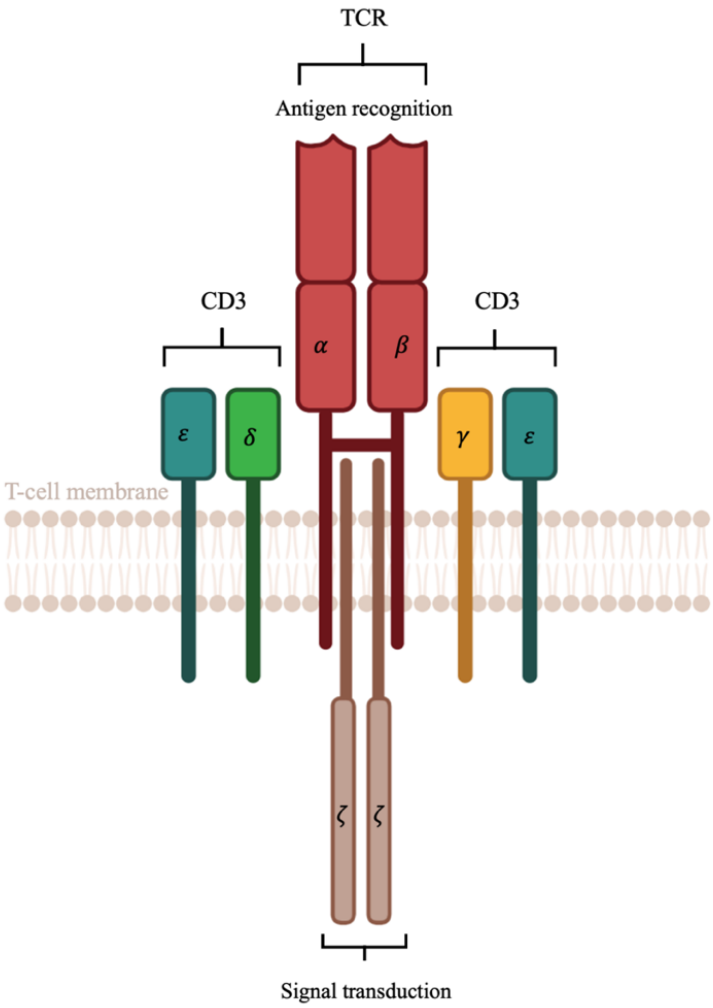

Figure 4: Cross-sectional view of TCR-CD3 complex on T-cell [26]

The TCR is responsible for Ag recognition consisting of a ligand-binding heterodimer with α and β chains. Whereas the CD3 complex is composed of a CDεδ heterodimer, a CDγε heterodimer and a ζζ homodimer responsible for signal transduction [27]. The process of signal transduction entails transmitting extracellular signals to induce intracellular responses, such as T-cell maturation or activation. The transmembrane proteins embedded in the membrane initiate the T-cell signal transduction pathways [27]. Three signals must be satisfied for T-cell activation to occur as illustrated in Figure 5.

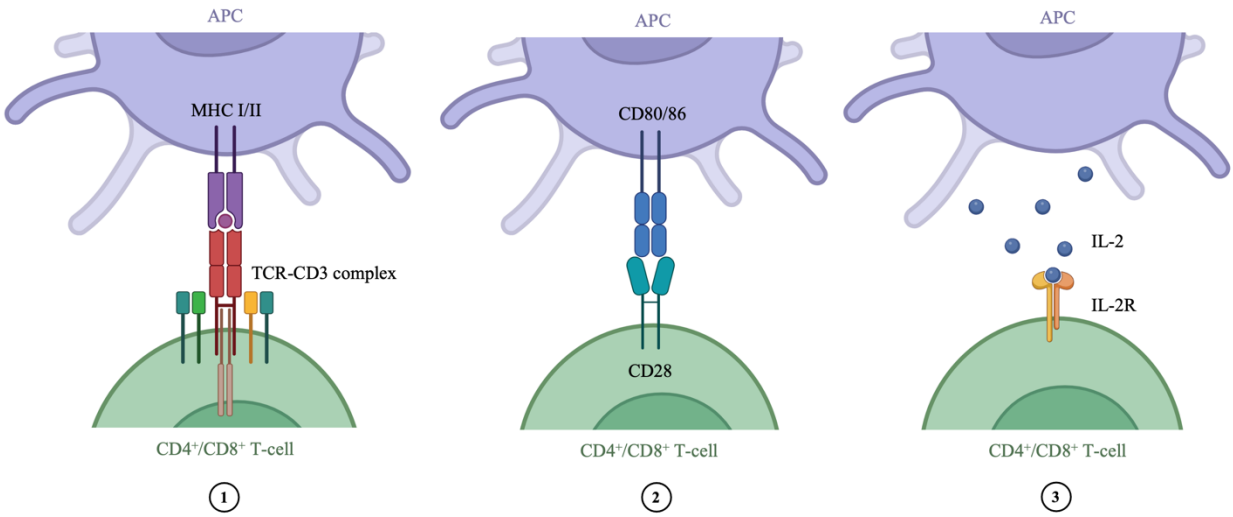

Figure 5: T-cell activation steps (1) Ag-specific recognition (2) Co-stimulation (3) Cytokine release [26]

(1) Ag-specific recognition: The first signal is initiated by the p(MHC) I or II of an APC stimulating the TCR-CD3 complex of a naïve CD_8^+ or CD_4^+ cell, respectively.

(2) Co-stimulation: The second signal is elicited by co-stimulatory molecules, such as CD28 on T-cells that bind to CD80 and CD86 presented on APCs.

(3) Cytokine release: The third signal secretes cytokines, namely the growth factor interleukin 2 (IL-2) and interferon-γ (IFN-γ) which promotes clonal expansion and activity of immune cells, respectively [23, 28]. T_{reg} cells engulf IL-2 produced by activated T-cells to suppress immune responses by limiting the nutrients required for T_{eff} cell proliferation [29].

Thirdly, activated T_c cells present the cancer-specific receptors suitable for cancer recognition and subsequent elimination.

2.2.2.2. Antigen-independent approach

Monoclonal antibodies are a subset of Abs commonly used in immunotherapy as an Ag-independent approach due to their high specificity [30]. Abs are a type of immunoglobulin (Ig) composed of two regions being the Fragment antigen binding (Fab) region and the Fragment crystallisable (Fc) region as displayed by Figure 6.

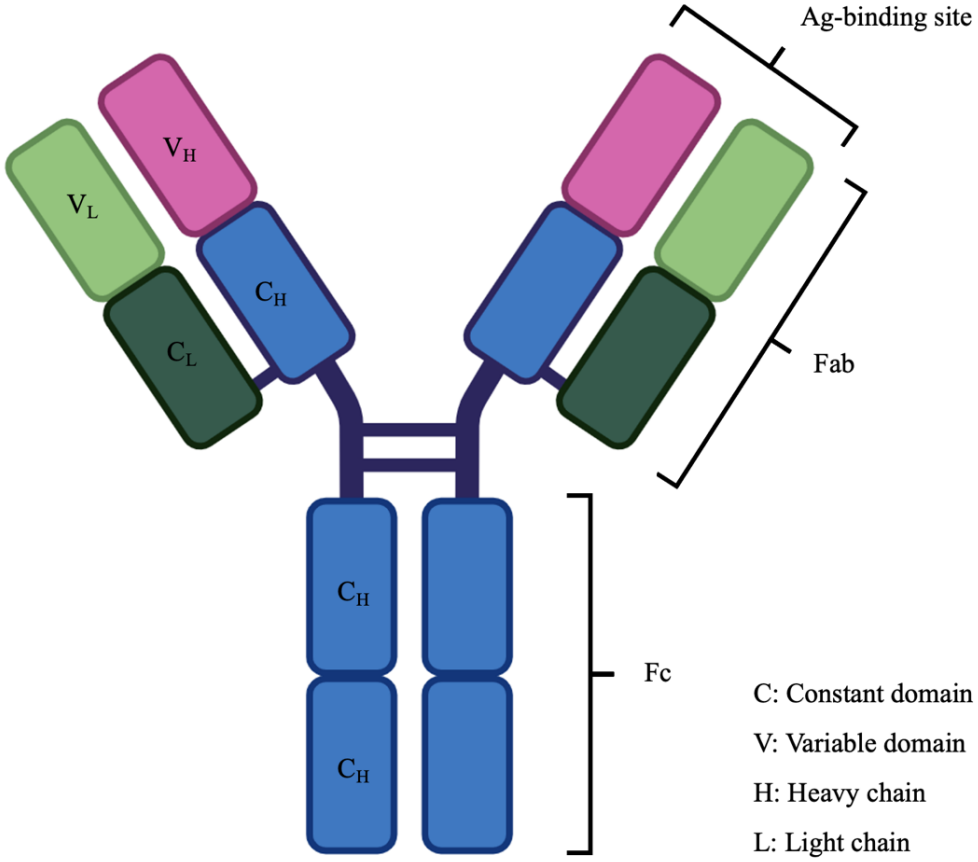

Figure 6: Structure of a monomer of Ig

The Fab region is the variable portion of the Ab and is responsible for Ag recognition. Whereas the Fc region is the constant portion that is recognized for its biological activity when interacting with specific receptors [31].

Abs and TCRs share similarities of being highly variable and having specific binding capabilities. They differ in that TCRs are bound to a membrane whereas Abs are free floating after being produced by B-cells. As mentioned previously, the CD3 complex in T-cells are essential in the activation of T-cells. Anti-CD3 mAbs can be used as non-physiological agonists in adoptive immunotherapy to induce the activation of T_{eff} cells. Thus, physiological responses resulting from an Ag-specific approach can be replicated using artificial agents like anti-CD3 mAbs. Anti-CD3 mAb mediated activation involves binding the CD3 integral protein to the Fc portion of an anti-CD3 mAb [32]. This Ag-independent approach can lead to the T_{eff} cells proliferating, differentiating, releasing cytokines, and eliminating cancer cells [33]. In addition to stimulating the activation of T_{eff} cells, Abs can recognize or inhibit the activity of T_{reg} cells. Target Abs with an affinity to T_{reg} cells can hinder the cells' ability to suppress the activation and proliferation of T_{eff} cells [34].

T-cells are mechanosensitive as mechanical forces influence their functionalities [35]. Shear stresses by fluid flow are applied on T-cells as they circulate in the peripheral blood. They also produce mechanical forces during the transmigration of T-cells which entails lymphocyte rolling, adhesion and migration into various tissues [36, 37]. Recent studies have been investigating the influence of mechanical forces on the efficacy of endogenous T-cell activation [38]. There are three factors that determine the extent of influence that mechanical forces have on a T-cell during activation. Namely, the strength of the TCR-pMHC signal, the ligand-binding spacing and the stiffness at the interface of the T-cell and the APC affect the strength of the T-cell activation. Weak mechanical forces are exerted on naïve T-cells when the TCR-pMHC signal is weak, the ligand spacing is large, and the surfaces are smooth. Conversely, strong mechanical forces are exerted on naïve T-cells when the TCR-pMHC signal is strong, the ligand spacing is small, and the surfaces

are rough. However, research relating to whether mechanical forces alone can activate T-cells remains dearth [39].

2.2.3. Adoptive T-cell therapy

ACT therapy relies on the body's existing immune system to provide a defence against cancer [3]. It follows a general sequence of events. The main types of ACT therapy are chimeric antigen receptor (CAR)-T-cell therapy, TCR T-cell therapy and tumour infiltrating lymphocytes (TIL) therapy.

1. **T-cell isolation:** Leukocytes (white blood cells) are isolated from the patient's peripheral blood by leukapheresis which provides access to circulating peripheral T-cells, which represent a fraction of the leukocytes. In TIL therapy, autologous tumour-specific T-cells (TILs) that live within the cancer are accessed by extracting them from fragments of the cancerous tumour.
2. **T-cell manipulation and expansion:** The different ACT techniques are illustrated in Figure 7.
    a) **CAR-T:** One or more genes that encode CAR specific to a target cancer Ag(s) is inserted in the T-cells to synthesize CAR-T-cells. The genes typically encode downstream intracellular signalling domains that allow CAR-T-cell to bypass the necessity of the MHC for endogenous T-cell activation [40].
    b) **TCR:** TCR-transduced T-cells are modified to recognize CAAs presented on the MHC of cancer cells [41].
    c) **TIL:** TILs recognize tumor-associated antigens (TAAs) and are expanded in cultures of IL-2 to support and promote T-cell proliferation. Tumour-specific recognition assays are used to evaluate their reactivity towards autologous tumours.

Following the selection, generation and manipulation of the above T-cells, they are expanded in vitro prior to infusion.

3. **T-cell re-infusion:** The modified and expanded T-cells are re-infused back into the patient's body with improved properties adequate to eliminate cancer cells.

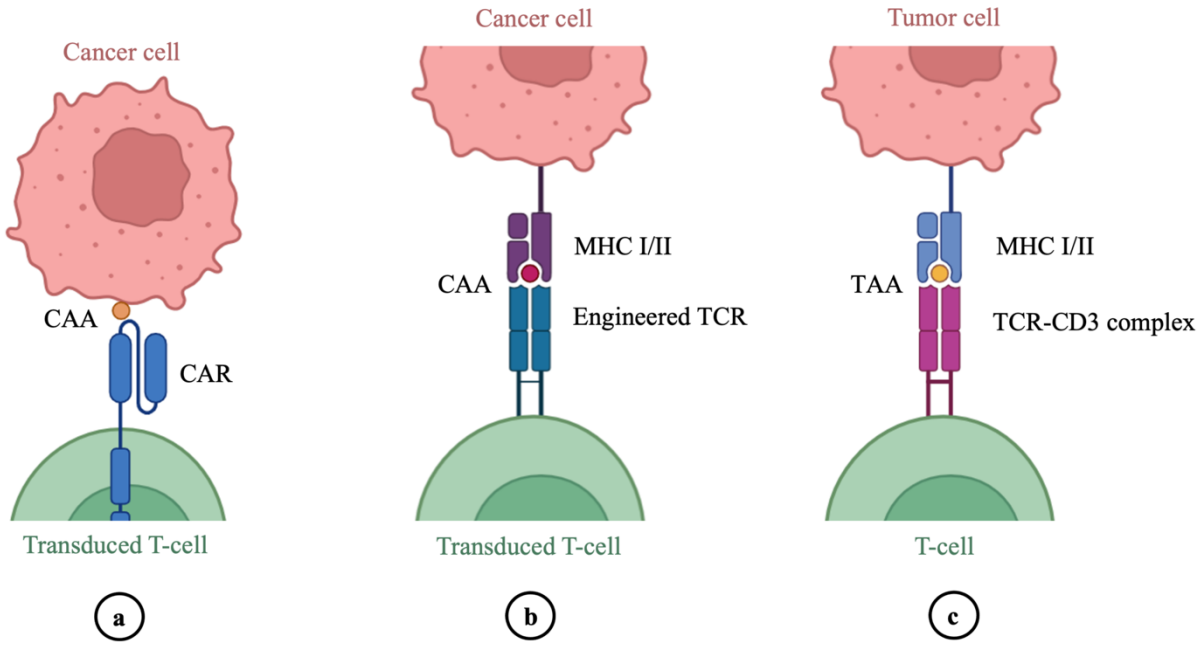

Figure 7: ACT immunotherapy techniques (a) CAR T (b) TCR (c) TIL [42]

ACT poses many advantages over conventional immunotherapy techniques that rely on the *in vivo* development of anticancer T-cells. It allows for the *in vitro* manipulation and expansion of the autologous T-cell in an environment that promotes its growth before being inserted into the body [3]. The current types of ACT rely on the use of indirect and direct methods of genetic and cellular engineering [43]. An *ex vivo* method in which physical means are employed is preferred as to avoid, reduce or complement the complexities associated with genetic and cellular engineering. The selective enhancement of T-cells by physically passing them through NH_2-MWCNT filters can be adapted into the ACT workflow to enhance its efficacy as a cancer treatment.

Chapter 3

3. Objectives

The aim of this master's project was to develop a MWCNT filter that possesses a dual functionality of both detaining immunosuppressive T-cells and inducing the activation of T_{eff} cells by mechanical forces and non-physiological agonists. To achieve this goal, the project was divided into 4 hypotheses as outlined by Figure 8 and Figure 9. The timeline of this master's project is also presented in Figure 8 which highlights the level of challenge associated to each hypothesis.

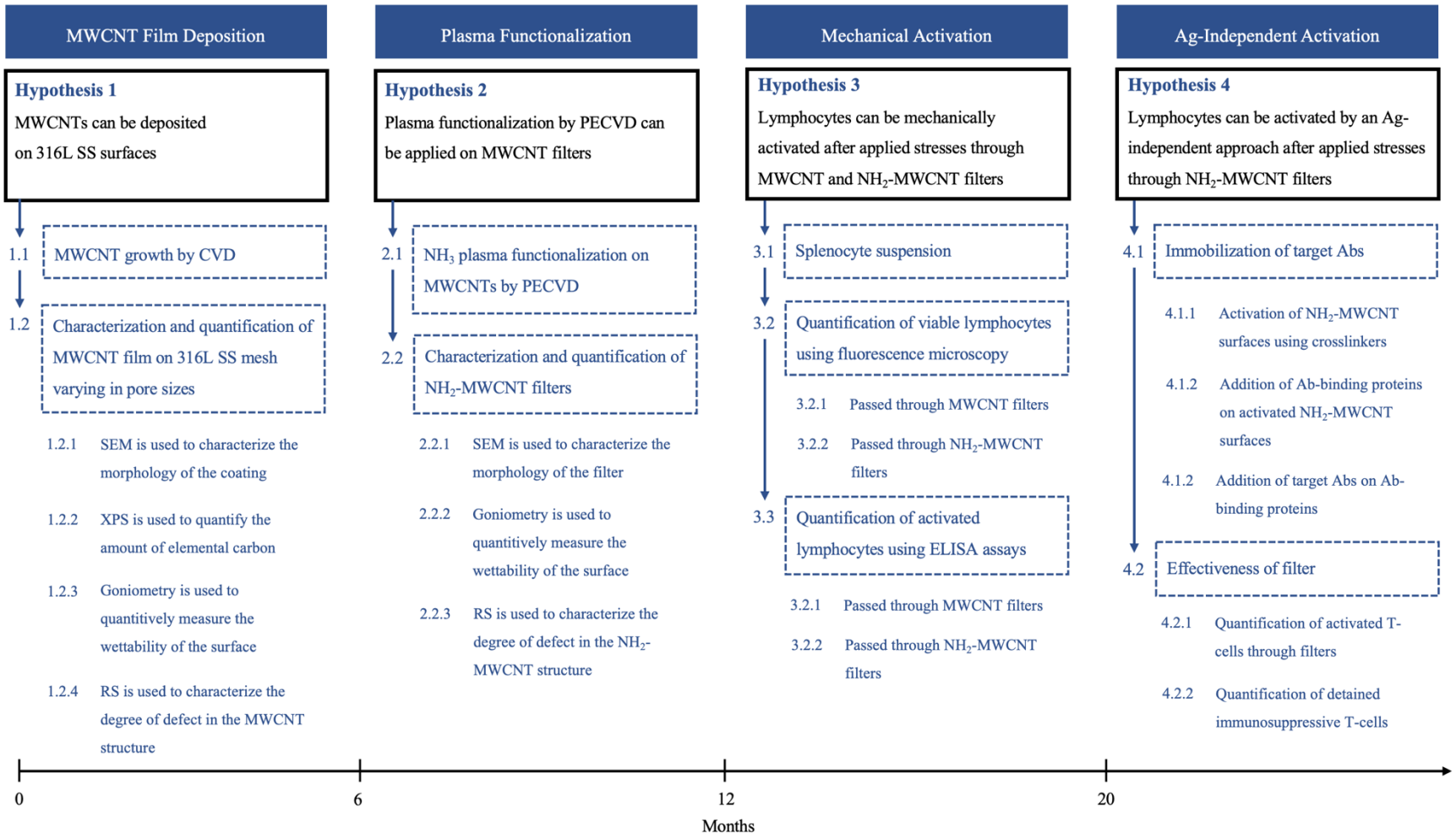

Figure 8: Outline of objectives and timeline

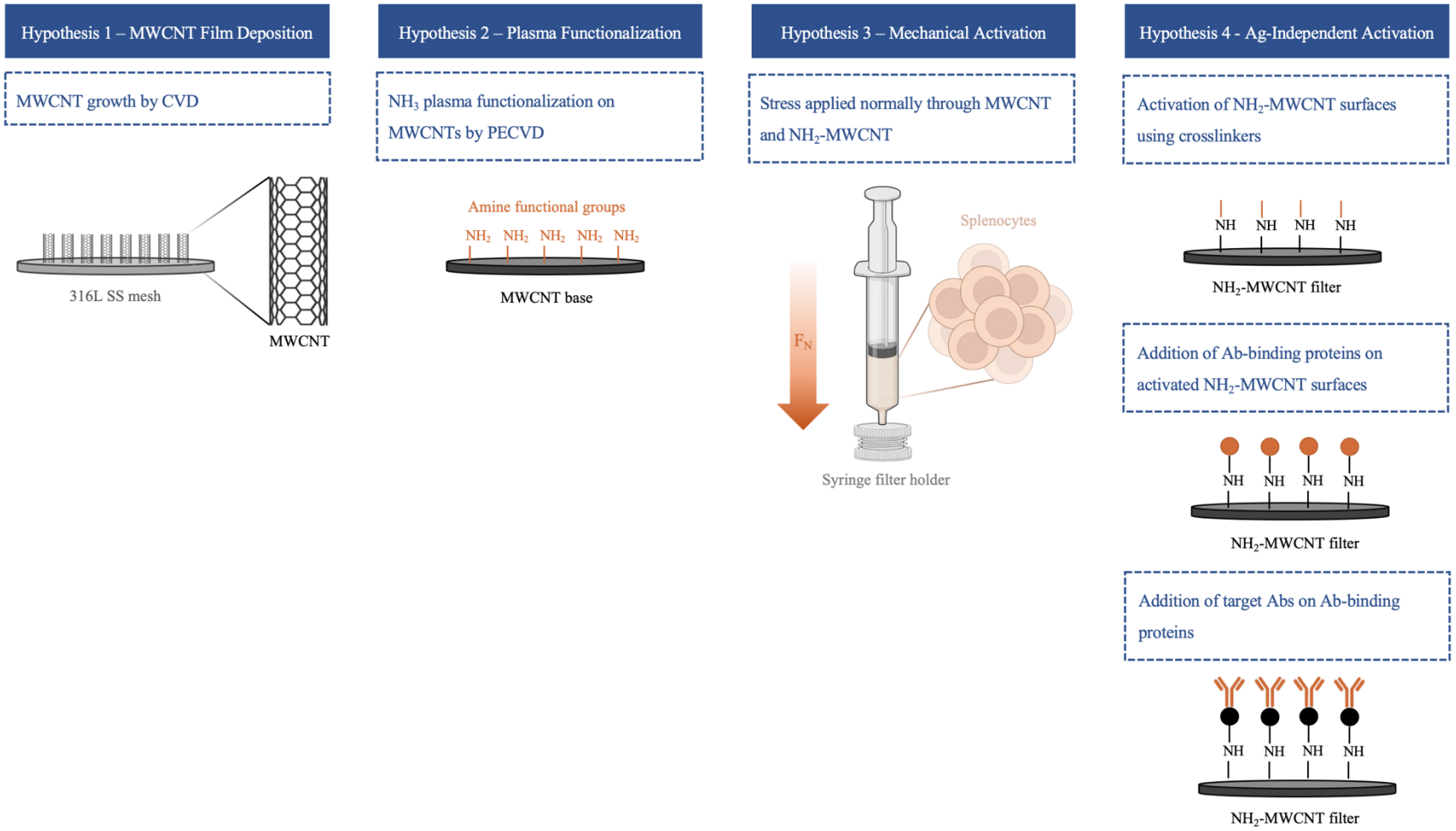

Figure 9: Visual representation of objectives

Chapter 4

4. Experimental methods

4.1. Filter fabrication

4.1.1. MWCNT synthesis on SS meshes

The technique of t-CVD was used to synthesize a homogenous coating of MWCNTs on metallic surfaces [44, 45]. MWCNTs were grown on different 316L SS meshes varying in grid opening sizes. The pore sizes were selected in reference to the typical diameters of murine lymphocytes. Therefore, lower and upper thresholds of 5 and 25 µm were chosen. The meshes were purchased from TWP Inc. and the product specifications are listed in Table 1.

Table 1: 316L SS product information

	1	2	3
Mesh size	200 × 1400 per 2.54 cm	165 × 1400 per 2.54 cm	80 × 700 per 2.54 cm
Wire diameter	71 × 41 µm	71 × 41 µm	102 × 76 µm
Opening size	5 µm	10 µm	25 µm
Overall thickness	0.15 mm	0.14 mm	0.28 mm
Weave type	Twill Dutch weave	Twill Dutch weave	Twill Dutch weave

This method required a gaseous hydrocarbon precursor in the presence of a catalyst on a substrate at elevated temperatures [45]. Acetylene (C_2H_2) acted as the hydrocarbon precursor. SS was an optimal choice of material as it acted as both the catalyst and the growth substrate which removed

the necessity of pre-treating the substrate with an external catalyst [46]. This was achievable due to its high iron content after a surface modification technique called oxidative heat treatment which promoted CNT growth [47, 48]. A standard operating procedure (SOP) for the synthesis of MWCNTs by t-CVD had been devised by the Catalytic & Plasma Process Engineering (CPPE) laboratory team at McGill University led by Jorge et al. [49]. This synthesis technique was developed and optimized for over more than a decade. A hammer-driven hole punch was used to cut circular samples with diameters of 2.38 cm out of the SS meshes. The SS samples were ultrasonically cleaned (Branson 5210) in acetone for 40 min.

Figure 10 and Figure 11 display the t-CVD setup and the block flow diagram of the system, respectively. An oxidative heat treatment step was performed which exposed the samples to air for 2 min in a furnace operating at a temperature of 700 ˚C (Thermo Scientific Lindberg/Blue M Split-Hinge Tube Furnace). The system was purged with argon (Ar) (Air Liquide, 99.999 %, 3148 sccm ± 5 sccm) for 4 min as to remove any residual air. Once the oxygen meter (Alpha Omega Instruments, Series 2000 Percent Oxygen Analyzer) read a value below 0.5 % (v %), Ar (592 ± 5 sccm) was introduced for 1 min. MWCNT growth was initiated by delivering C_2H_2 (Air Liquide, 99.6 %, 68 sccm ± 5 sccm) to the system concurrent to the Ar flow (592 ± 5 sccm) for 2 min. The flow of C_2H_2 was then stopped while the Ar continued to flow (592 ± 5 sccm) for another 2 min which allowed the samples to rest at 700 ˚C. The system was purged with Ar (3148 sccm ± 5 sccm) for 5 min after which the MWCNT-coated SS samples were removed. Hereinafter, the MWCNT-coated SS samples are referred to as MWCNT filters.

Figure 10: Side view of the t-CVD setup in the CPPE laboratory (1) Loading chamber (2) Elephant trunk hose (3) Gas exhaust valve (4) Furnace control panel (5) Furnace tube (6) Gas flow inlet (7) Wire to pull Quartz boat

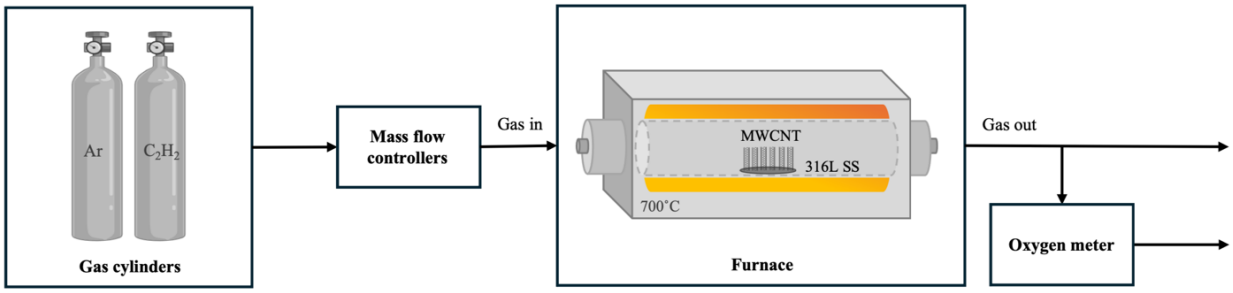

Figure 11: Block flow diagram of t-CVD system

4.1.2. Plasma functionalization on MWCNT filters

Plasma-enhanced chemical vapour deposition (PECVD) was used to graft amine functional (R-NH_2) groups on the MWCNT filters. A SOP for the plasma functionalization of MWCNTs yielding a high quantity of amine functional groups has been reported by Hein et al. in the CPPE laboratory team at McGill University [50]. The system consisted of a capacitively-coupled radiofrequency (RF) plasma reactor capable of operating at sub-atmospheric pressures with various plasma-forming gases. The power supply and matching network (RFX600A, Advanced Energy) provided a 13.56 MHz continuous-wave excitation of the plasma. Figure 12 and Figure 13 display the PECVD setup and the block flow diagram of the system, respectively. The plasma was sustained between two parallel disk SS electrodes that measured 10 cm in diameter and separated by 1.5 cm. A quartz disk with a thickness of 3.5 mm rested on top of the bottom RF energized electrode.

The reactor was first evacuated to a low pressure (Leybold TRIVAC® T pump, 5 mTorr base pressure) and subsequently purged with Ar (Air Liquide, 99.999 %, 2279 sccm ± 5 sccm) for 3 min to remove residual air. The SS-supported MWCNT filters were subjected to an argon plasma pre-treatment process in which Ar plasma (250 sccm ± 5 sccm, 30 W) was sustained between the disk electrodes for 10 min. The necessity of the Ar pre-treatment was reported by Hein et al. [50]. Ammonia (NH_3) (Specialty Gases of America Inc., 99.99 %) was used as the source of reactive species to attach R-NH_2 groups onto the filters. The filters were exposed to NH_3 plasma (10 sccm ± 5 sccm, 5 W) for 45 min. The filters rested in the low-pressure system for 10 min to stabilize the active sites. The system was purged with Ar (2279 sccm ± 5 sccm) for 10 min after which the NH_2-MWCNT filters were removed. The top of the MWCNT surface that is primarily exposed to the NH_3 plasma is the NH_2-functionalized side.

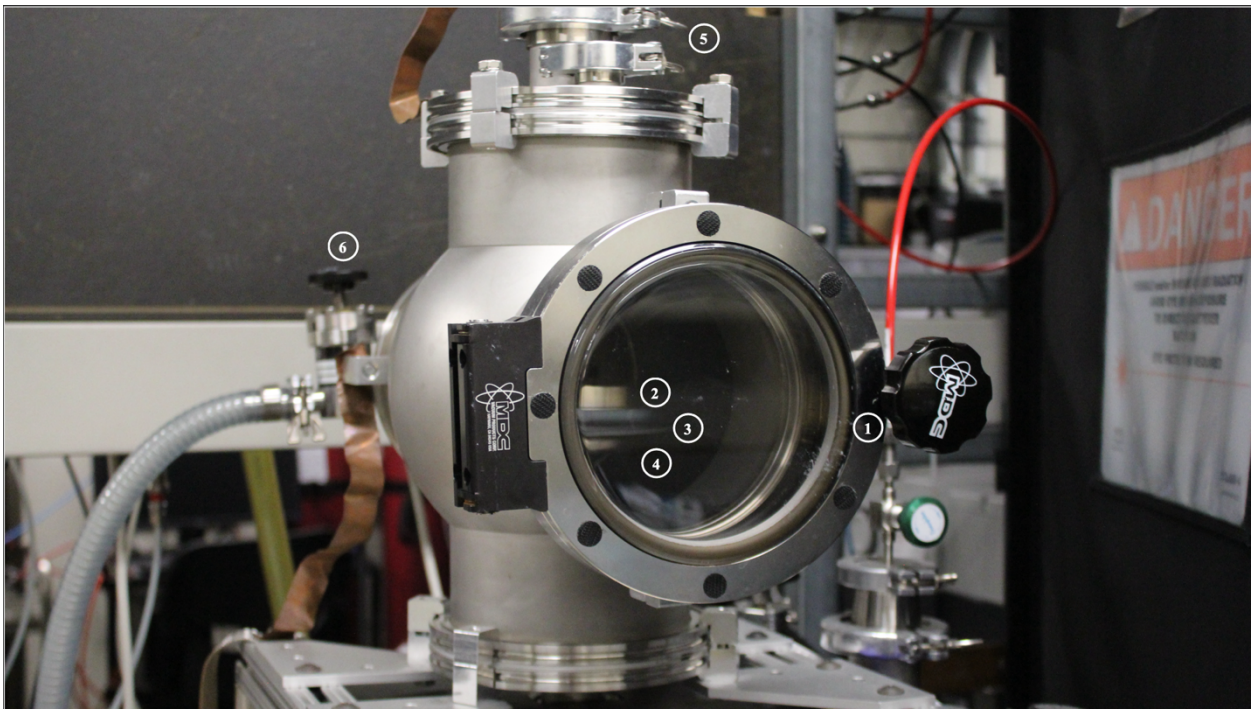

Figure 12: Photograph of PECVD setup in the CPPE laboratory (1) Chamber door (2) Ground electrode (3) Quartz disk (4) RF electrode (5) Gas flow inlet (6) Vacuum pump pin valve

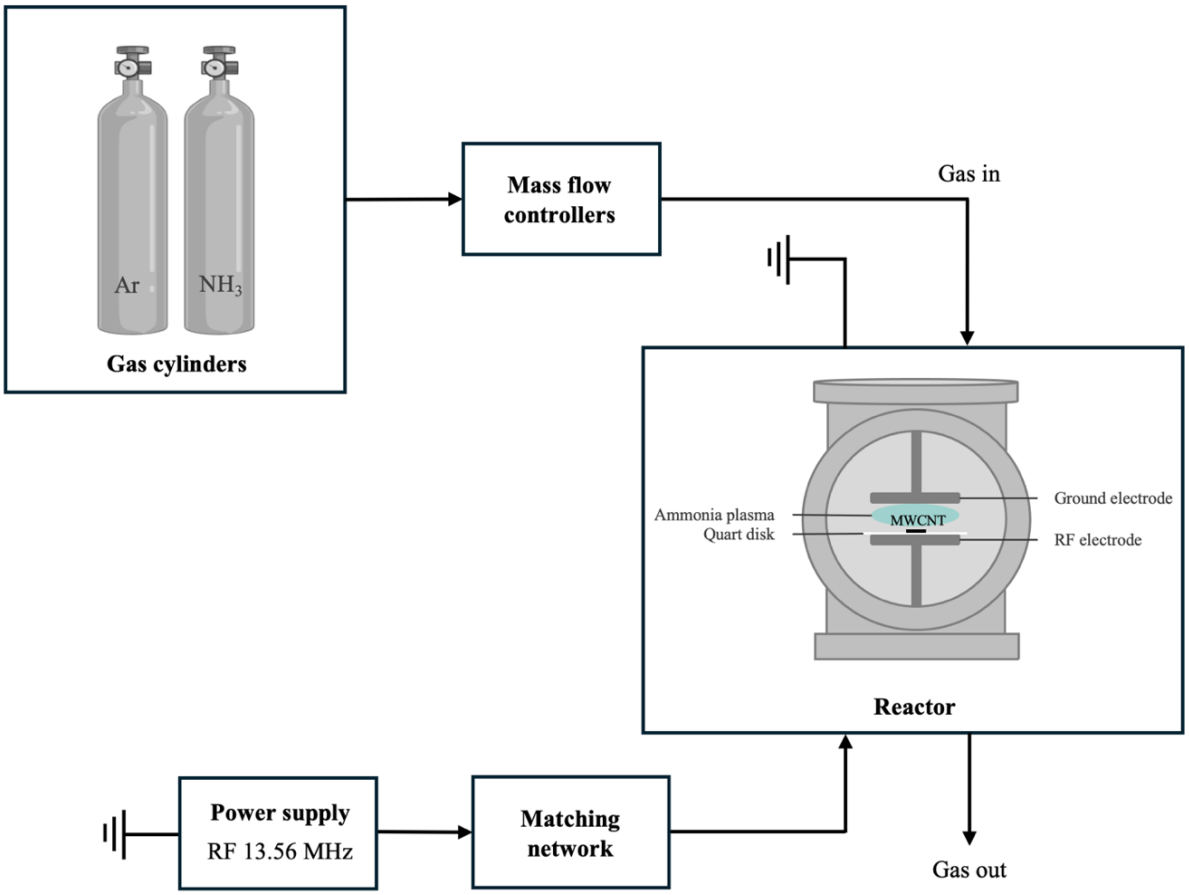

Figure 13: Block flow diagram of PECVD system

4.1.3. Surface characterization

Circular samples with diameters of 2.38 cm were cut out of the SS mesh and ultrasonically cleaned (Branson 5210) in acetone for 40 min. The weaving pattern of the 316L SS mesh with varying grid opening sizes were analyzed using scanning electron microscopy (SEM) (Hitachi, SEM SU3500) with an accelerating voltage of 10 kV. The SEM SU3500 under the same operating conditions was also used to investigate the surface morphology of the MWCNT filters before and after NH_3 plasma treatment.

Static water contact angle (WCA) measurements were performed using the optical contact angle (OCA) goniometer (DataPhysics, OCA 15EC) to determine the hydrophobicity of the SS material. Four water droplets of 5 µL were dispensed (Hamilton 500 µL syringe) horizontally along the radius of hydrophobic surfaces, whereas two water droplets of 5 µL were dispensed onto hydrophilic surfaces. The measurable surface area became limited once the filter was saturated with water. The Young-Laplace equation was used as the best fit model for the drop analysis.

X-ray photoelectron spectroscopy (XPS) (Thermo Scientific Nexsa G2 Surface Analysis System) with a source analysis diameter of 400 µm was used to determine the elemental compositions on the surface of the MWCNT film. The pressure in the analysis chamber was maintained under $3.75E^{-7}$ Torr.

Raman spectroscopy (Thermo Scientific DXR2 Raman Microscope) with a 532 nm excitation laser at a power of 4 mW was used to determine the level of defect in the structures of the MWCNT and NH_2-MWCNT filters. The Raman spectrum was obtained for five different points selected on the surface of the filters and overlayed to display a combined Raman spectrum.

4.2. Lymphocyte interaction

4.2.1. Splenocyte suspension

A C57BL/6J mouse was euthanized using isoflurane while respecting the CR-CHUM comité institutional de protection des animaux (CIPA) guidelines. Prior to euthanasia, the mice lived in sterile cages in ventilated racks with a bedding material composed of hardwood beta chips. The mice had access to water by an automated water system which was sterilized before their consumption. They followed the 2018 Teklad global rodent diets [51].

A spleen was collected into a sterile petri dish containing 1× Dulbecco's phosphate buffered saline (D-PBS) (Wisent Inc., without calcium and magnesium) solution and kept on ice until manipulation. A single-cell C57BL/6J murine spleen suspension was created under a biological safety cabinet (Microzone Corpororation, Bio-Klone 2) by compressing the spleen between two frosted glass slides. The glass slides were washed with 30 mL of D-PBS and filtered through a 70 µm cell strainer atop of a 50 mL conical tube. The suspension was evenly distributed into two 15 mL conical tubes and centrifuged (Heraeus Instruments, Baxter Megafuge 1.0 Centrifuge) at 1500 RPM for 5 min which sedimented the cells into a pellet. The supernatant was discarded while the pellet was resuspended in 5 mL of 1× red blood cell (RBC) lysis (Thermo Fischer Scientific, Invitrogen) and kept on ice for 5 min. The RBC lysis allowed for the isolation of white blood cells (WBCs) in the spleen, or splenocytes by removing the RBCs in the suspension. The suspension was centrifuged at 1500 RPM for 5 min. Each pellet was resuspended into 5 mL of PBS and kept on ice until used. Spleens aid in immune responses as they contain white blood cells. Therefore, the suspension of splenocytes with a concentration of $5E10^6$ cells/mL provides access to T-cells.

The chamber of a cell counting slide was loaded with 5 µL of the suspension and 5 µL of trypan blue. The slide placed inside an automated cell counter (TC20™ Automated Cell Counter, Bio Rad) to determine the cell concentration.

4.2.2. Splenocyte suspension through MWCNT and NH_2-MWCNT filters

A positive control was prepared in which a microtube was filled with 1 mL of splenocyte suspension and heated to 95 ˚C for 10 min to kill the cells in suspension. MWCNT and NH_2-MWCNT filters varying in grid opening sizes (5, 10 and 25 µm) were encased in separate syringe filter holders (Fischer Scientific, Sartorius Syringe Filter Holders). A suspension of 1.5 mL was dispensed normally using a 10 mL syringe through each filter into individual wells of a multiwell cell culture plate. The syringe was subjected to the arbitrary force exerted by the researcher. The filtered suspensions were transferred into separate microtubes. The experimental setup for filtering the splenocyte suspension is displayed in Figure 14.

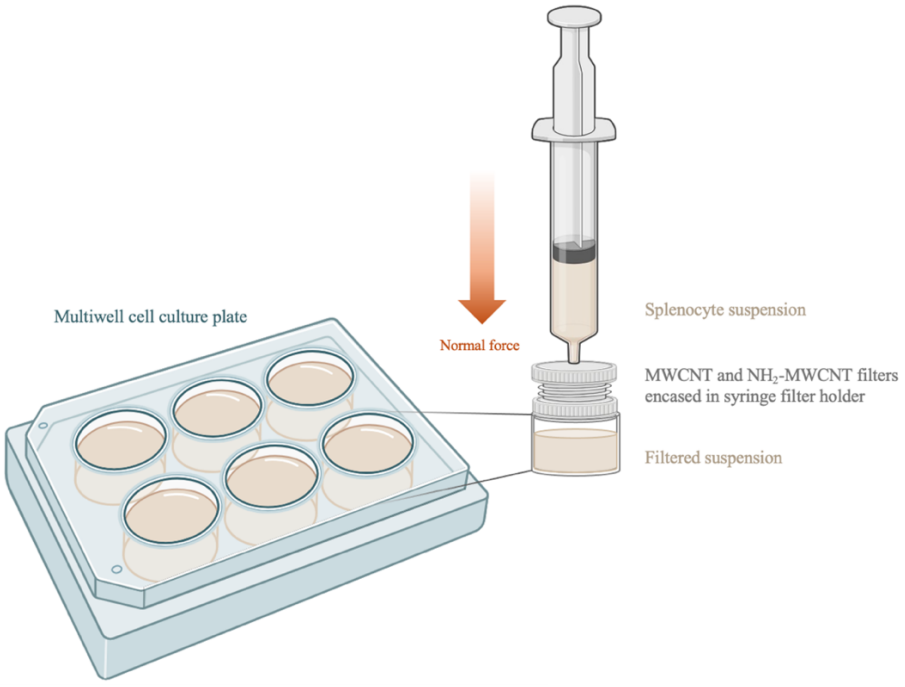

Figure 14: Setup for filtering splenocyte suspension through MWCNT and NH_2-MWCNT filters

4.2.3. Spleen cell viability

Calcein-acetoxymethyl (AM) (Thermo Fischer Scientific, Invitrogen) was used as the fluorescent indicator for assessing cell viability in the filtered splenocyte suspensions after being filtered through the MWCNT and NH_2-MWCNT filters. Calcein-AM is membrane permeable and converts the live cells fluorescent green after intracellular esterases hydrolyse AM esters [52]. 5 µM of calcein-AM was added to every microtube containing the splenocyte suspension. The suspensions were incubated at 37 ˚C (Fisher Scientific, Isotemp® Water-Jacketed Incubator, 5.5 % CO_2) for 1.5 hrs, then centrifuged (Thermo Fischer Scientific, Sorvall™ Legend™ Micro 17 Microcentrifuge) at 1500 RPM for 5 min. The pellet was resuspended in 1 mL of D-PBS and incubated at 37 ˚C for 30 min. The suspensions were transferred from microtubes to separate wells of a multiwell cell plate. Fluorescence microscopy was immediately performed after. The fluorescence microscope (Thermo Fischer Scientific, Invitrogen™ EVOS™ FL Imaging System) was equipped with different fluorescence channels. The transmitted light (TL) and green fluorescent protein (GFP) channels were used to determine the viability of spleen cells after being passed normally through the MWCNT and NH_2-MWCNT filters. The spleen cell viability experiments were repeated three times to ensure the repeatability of the results.

ImageJ was used to process the images and determine the cell count for the given field of view (FOV). The sizes of particles included in the cell count ranged between 4 pixel^2 to infinity pixel^2 required a circularity of at least 40%.

A single factor analysis of variance (ANOVA) test was conducted to determine whether there were statistically significant differences in the viability cells after filtration. The threshold for a significance value was selected to be <0.05.

4.2.4. Enzyme-linked immunosorbent assay

The activation of T-cells after filtration was assessed using the mouse IFN-γ ELISA kit (Thermo Fischer Scientific, Invitrogen Catalog # KMC4021) which quantified the amount of IFN-γ secreted in the supernatant of the splenocyte suspension. The kit included pre-coated wells in a 96-well plate with the capture antibody specific to mouse IFN-γ.

Three independent splenocyte through MWCNT and NH_2-MWCNT filters experiments were carried out. The samples were stored at a temperature of -18 ˚C before performing the assay once with duplicates. Before preforming the ELISA procedure, the filtered splenocyte suspension samples required preparation. The samples were centrifuged (Thermo Fischer Scientific, Sorvall™ Legend™ Micro 17 Microcentrifuge) at 1500 RPM for 5 min. The pellet was discarded while the supernatant was transferred into new microtubes.

A positive control was prepared to stimulate the secretion of IFN-γ. It consisted of adding 2 µL of phytohemagglutinin-L (PHA-L) (500×) (eBioscience™ Invitrogen™, Thermo Fischer Scientific) to splenocytes suspended in 1 mL of 1× Roswell park memorial institute (RPMI) 1640 (Wisent Inc., without L-glutamine and sodium pyruvate) enriched with 10 % heat inactivated fetal bovine serum (FBS) (Wisent Inc.), 1 % penicillin-streptomycin (Thermo Fischer, Gibco™), 50 µM 2-mercaptoethanol (Thermo Fischer, Gibco™), 1 % L-glutamine (Thermo Fischer, Gibco™), 1 mM sodium pyruvate (Thermo Fischer, Gibco™), and 0.1 mM minimum essential medium (MEM) non-essential amino acids (Thermo Fischer, Gibco™). The positive control was incubated for 48 hrs at 37 ˚C (Fisher Scientific, Isotemp® Water-Jacketed Incubator, 5.5% CO_2) to allow adequate time to produce cytokines.

The IFN-γ standards were prepared by performing seven serial dilutions. The mouse IFN-γ standard was diluted with the standard dilution buffer to a concentration of 3000 pg/mL. The diluted standard solution was added to the standard diluent buffer to create standard solutions of mouse IFN-γ with concentrations of 300, 150, 75, 37.5, 18.8, 9.4, 4.7, and 0 pg/mL.

Table 2: List of buffers and reagents

Chemicals
Mouse IFN-γ biotin conjugate
Mouse IFN-γ standard
Wash buffer concentrate (25×)
Standard diluent buffer
Streptavidin-horseradish peroxidase-(HRP) (100×).
Streptavidin-HRP diluent
Stabilized chromogen, tetramethylbenzidine (TMB)

The ELISA procedure was divided into five sections and represented in a schematic by Figure 15.

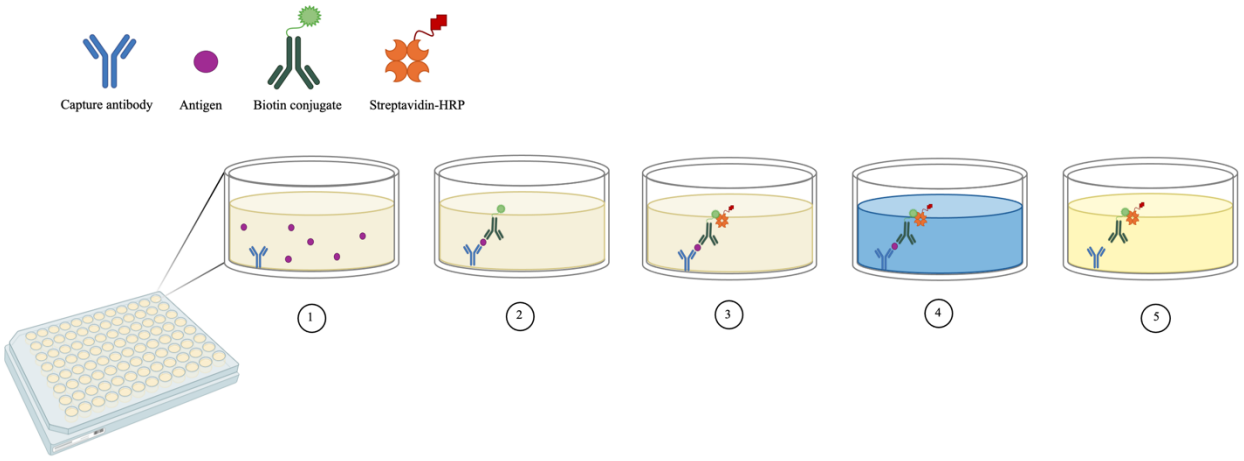

Figure 15: Visual representation of ELISA steps

(1) Binding of Ag: 100 µL of standards, controls and samples were added into separate wells of the plate. The wells for chromogen blank were left empty. The 96-well plate was covered with an adhesive plate cover and kept at room temperature in a dark environment for 2 hrs. The solution inside of the wells was discarded and rinsed with 1× wash buffer.

(2) Addition of biotin conjugate: 100 µL of mouse IFN-γ biotin conjugate was added into each well previously bound to the Ag. The plate was covered with an adhesive plate cover and kept at room temperature in a dark environment for 1 hr. The solution inside of the wells was discarded and rinsed with 1× wash buffer.

(3) Addition of streptavidin-HRP: 100 µL of 1× streptavidin-HRP was added into each well previously bound to the biotin conjugate. The plate was covered and kept at room temperature in a dark environment for 30 min. The solution inside of the wells was discarded and rinsed with 1× wash buffer.

(4) Addition of stabilized chromogen: 100 µL of stabilized chromogen to each well including the chromogen blanks. The plate was covered and kept at room temperature in a dark environment for 30 min. The color of the solution in the wells changed to blue.

(5) Addition of stop solution: 100 µL of stop solution was added to each well such that the color of the solution in the wells changed from blue to yellow.

The plate was read with a microtiter plate reader (Thermo Scientific, Varioskan LUX Multimode Microplate Reader) at an absorbance of 450 nm within 2 hrs of adding the stop solution. The standard solutions with known concentrations of mouse IFN-γ were used to generate the standard curve. The chromogen blank absorbances were subtracted from the unknown concentration absorbances to remove background interference.

Chapter 5

5. Results and discussion

5.1. Surface characterization

5.1.1. Pristine SS mesh

5.1.1.1. Scanning electron microscopy

Figure 16 (a-c) shows SEM images of the 316L SS mesh after ultrasonic cleaning. The high-magnification imaging captured the interwoven pattern of the SS mesh and the pristine nature of the base material. As MWCNT synthesis by t-CVD is a surface-specific technique that relies on the quantity of catalytic nanoparticles at the surface, the material composition is important. The SS wires in Figure 16 (a-c) were woven in a Twill Dutch pattern and were composed of the same material being the 316L SS. Therefore, the different pore size of the SS mesh was the only variable being investigated. The dark regions between the twisted wires were the grid opening sizes where the T-lymphocytes passed through the filters.

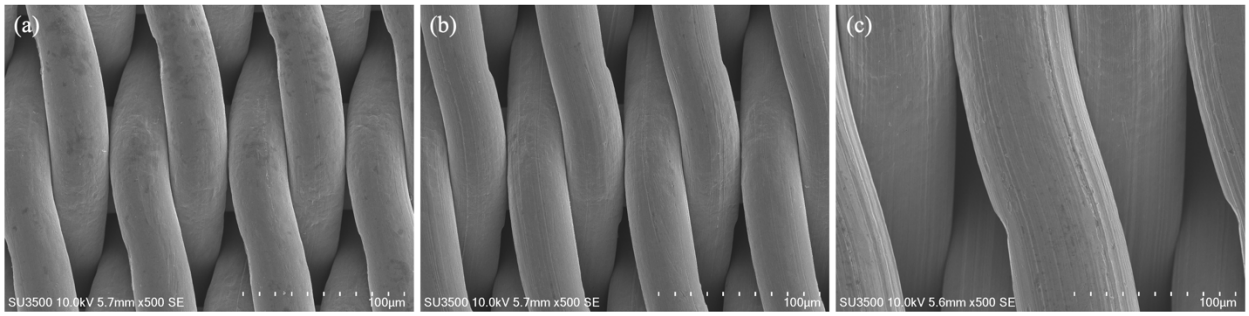

Figure 16: SEM images of pristine 316L SS mesh of varying pore sizes (a) 5 µm (b) 10 µm (c) 25 µm

5.1.1.2. Water contact angle

Figure 17 (a-c) displays the 5 µL dispended water droplet on the pristine 316L SS mesh of varying grid opening sizes. Both the 10 and 25 µm SS meshes were slightly hydrophobic as the WCA was greater than 90˚ being 115.7˚ and 90.9˚, respectively. The 5 µm SS mesh was slightly hydrophilic as the WCA was less than 90˚ being 82.9˚.

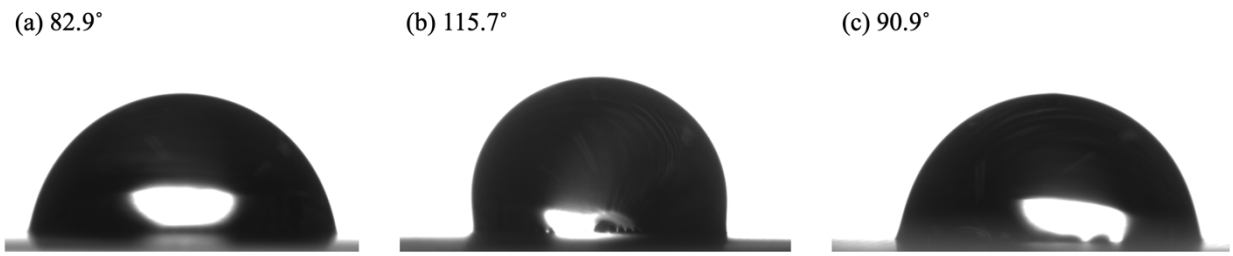

Figure 17: WCAs of pristine 316L SS mesh of varying pore sizes (a) 5 µm (b) 10 µm (c) 25 µm

5.1.2. MWCNT

5.1.2.1. Scanning electron microscopy

Figure 18 (a), (b) and (c) show the MWCNT coated SS mesh with grid opening sizes of 5, 10 and 25 µm, respectively. A forest-like network of MWCNTs was synthesized and coated homogenously on the 316L SS mesh. The MWCNTs were evenly distributed across the surfaces of the meshes of varying pore sizes. Therefore, the different pore sizes did not influence the yield of the MWCNT synthesis by t-CVD.

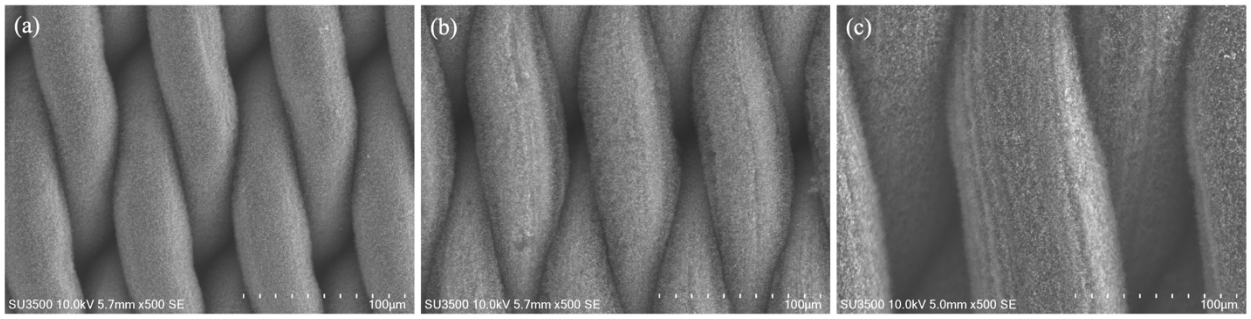

Figure 18: SEM images of MWCNT filters (a) 5 µm (b) 10 µm (c) 25 µm

Figure 19, Figure 20 and Figure 21 display SEM images of the 5, 10 and 25 µm MWCNT filters with ranging magnifications, respectively. At higher magnifications, the individual long tubular cylinders and their alignment on the SS surface become visible.

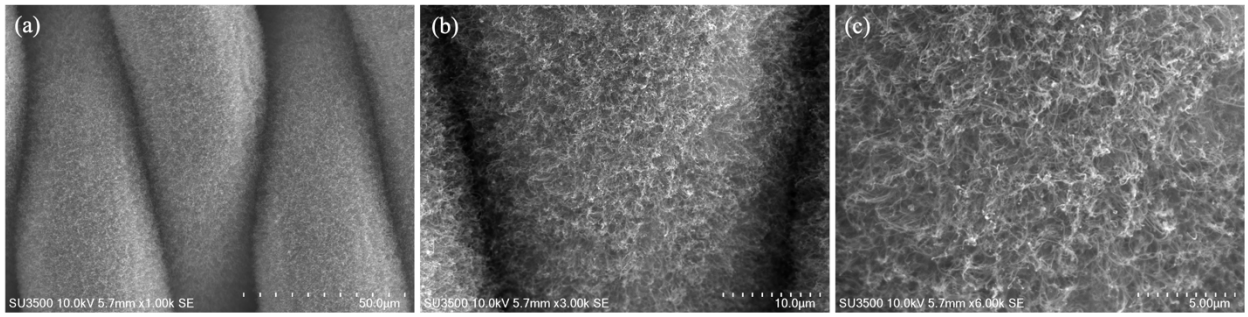

Figure 19: SEM images of 5 µm MWCNT filters at different magnifications (a) ×1000 (b) ×3000 (c) ×6000

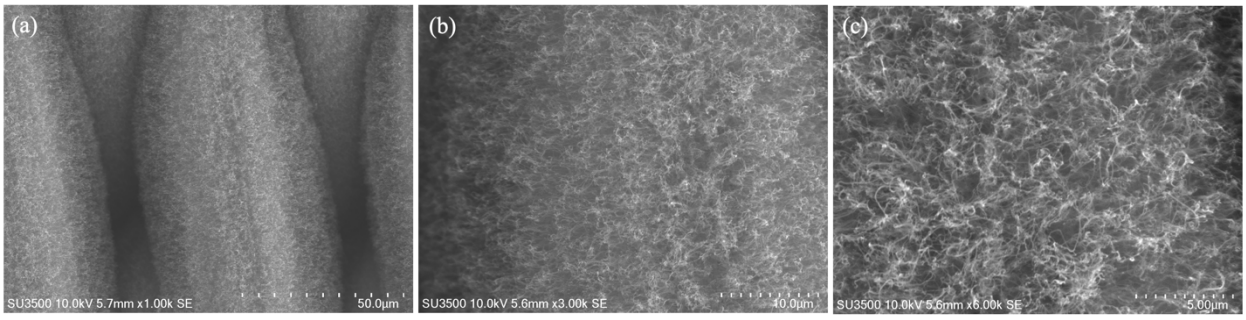

Figure 20: SEM images of 10 µm MWCNT filters at different magnifications (a) ×1000 (b) ×3000 (c) ×6000

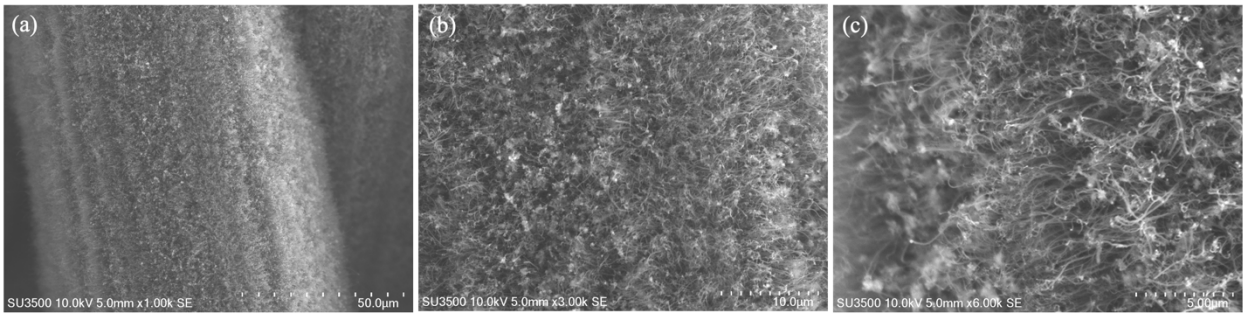

Figure 21: SEM images of 25 µm MWCNT filters at different magnifications (a) ×1000 (b) ×3000 (c) ×6000

5.1.2.2. Water contact angle

Figure 22 (a-c) displays the 5 µL dispended water droplets on the MWCNT filters of the varying pore sizes. All the MWCNT surfaces exhibited hydrophobic properties as the WCAs for the 5, 10, 25 µm filters were 151.3˚, 157.0˚ and 143.7˚, respectively. Both the 5 and 10 µm MWCNT filter were superhydrophobic as their WCAs were greater than 150˚. The 25 µm MWCNT filter was not considered superhydrophobic. The lower WCA could be attributed to the capillary and gravitational effect of the water droplet through the mesh given its larger pore size.

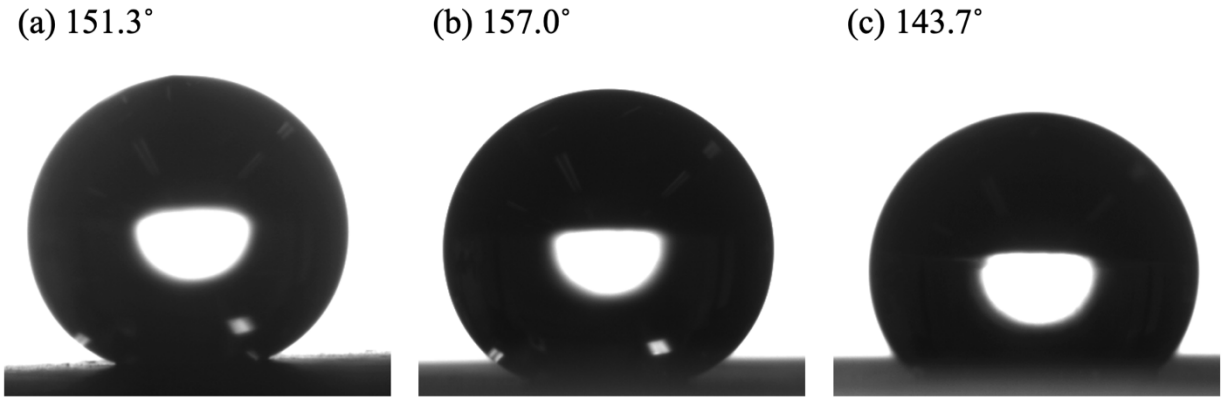

Figure 22: WCAs of MWCNT filters (a) 5 µm (b) 10 µm (c) 25 µm

5.1.2.3. X-Ray photoelectron spectroscopy

The XPS survey spectra in Figure 23, Figure 24 and Figure 25 are overlays of the survey scans. They indicated the presence of carbon (C) and oxygen (O) on the surface of the MWCNT filters. The Thermo Scientific Avantage software automatically identified elements in the survey spectrum. The MWCNTs were high in purity as they contained 98.8 %, 98.7 % and 99.2 % of C for the 5 µm, 10 µm and 25 µm filters, respectively. The quantity of O detected on the surface was insignificant and likely due to oxidation from the exposure to ambient air after MWCNT synthesis.

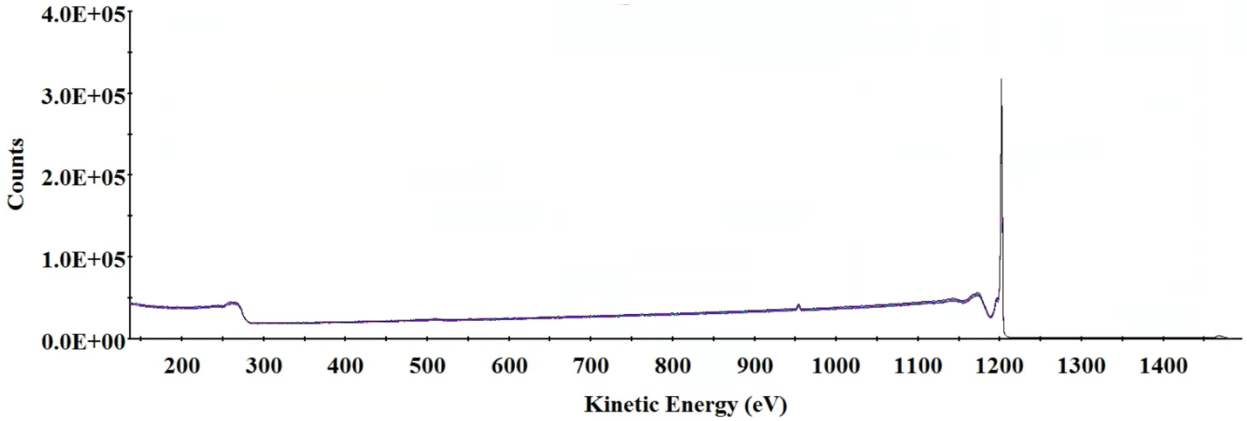

Figure 23: XPS survey scans of 5 µm MWCNT filters

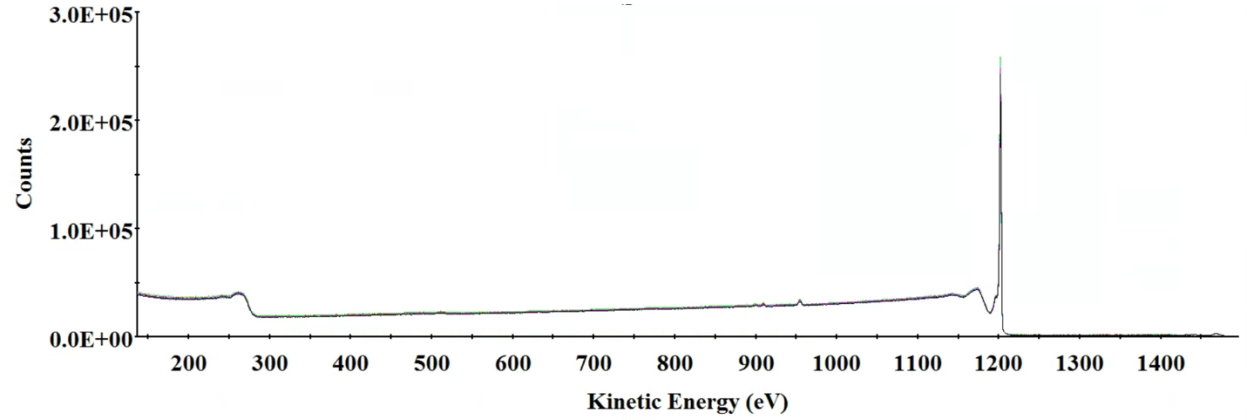

Figure 24: XPS survey scans of 10 µm MWCNT filters

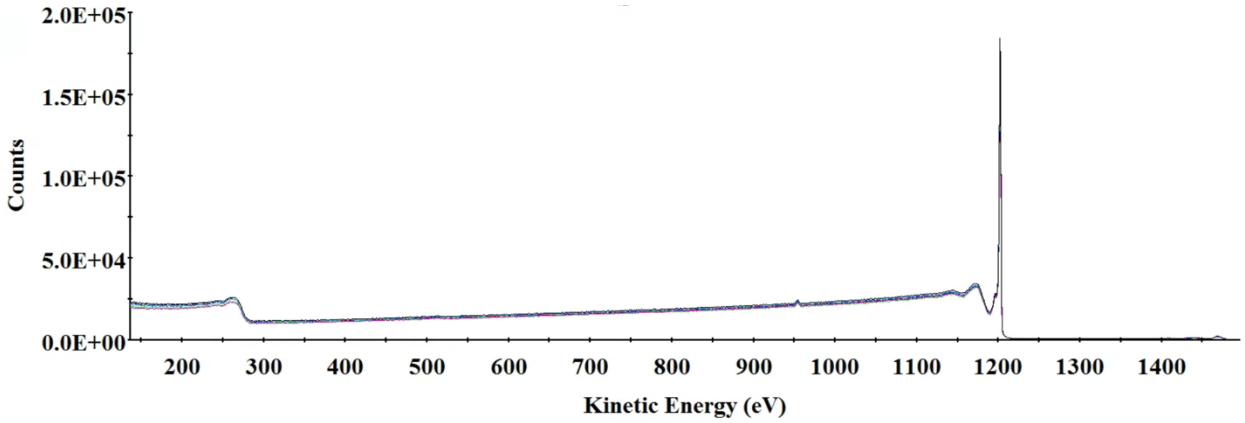

Figure 25: XPS survey scans of 25 µm MWCNT filters

5.1.2.4. Raman spectroscopy

The Raman spectra for the 5, 10 and 25 µm MWCNT filters are displayed by Figure 26, Figure 27 and Figure 28, respectively. Characteristic to MWCNTs, the filters share peaks with Raman shifts at 1350 cm^{-1} (D-band) and 1585 cm^{-1} (G-band). The Raman spectrum is the structural fingerprint which reveals the vibrational modes of the carbon atoms within the MWCNT sample [53]. The G-band corresponds to in-plane stretching of carbon atoms while the D-band represents the defects in the sp^2-hybridized carbon atoms in graphite. The D band and G band intensity ratio (I_D/I_G) is an indicator of the induced structural disorder. The I_D/I_G ratio was used to compare the proportions of sp^2 and sp^3 sites after NH_3 plasma functionalization.

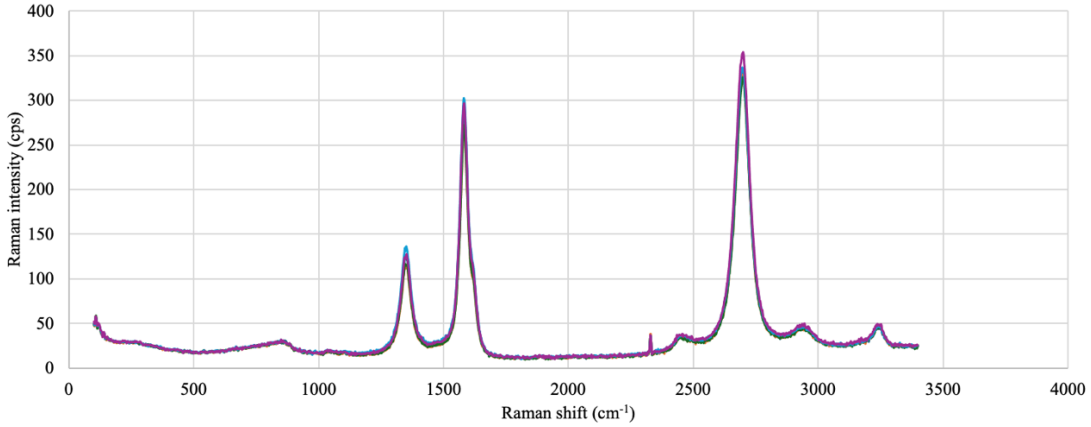

Figure 26: Raman spectra of 5 µm MWCNT filters

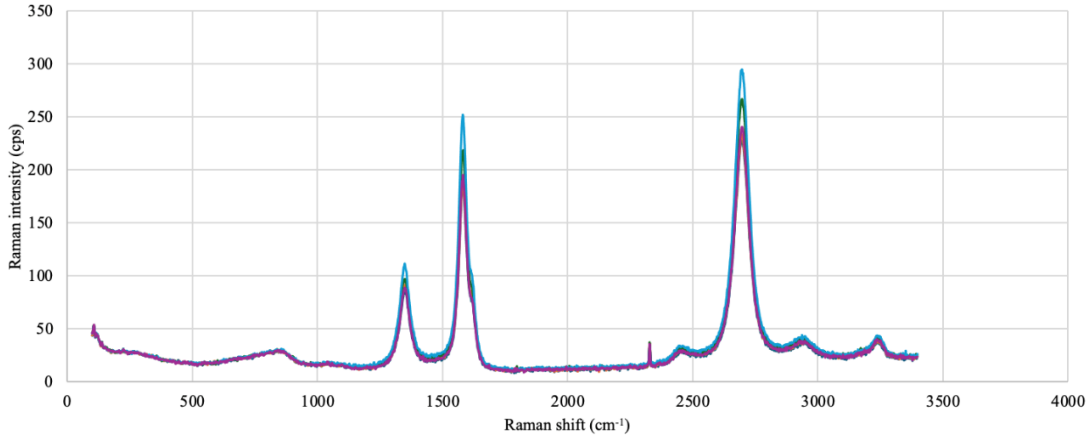

Figure 27: Raman spectra of 10 µm MWCNT filters

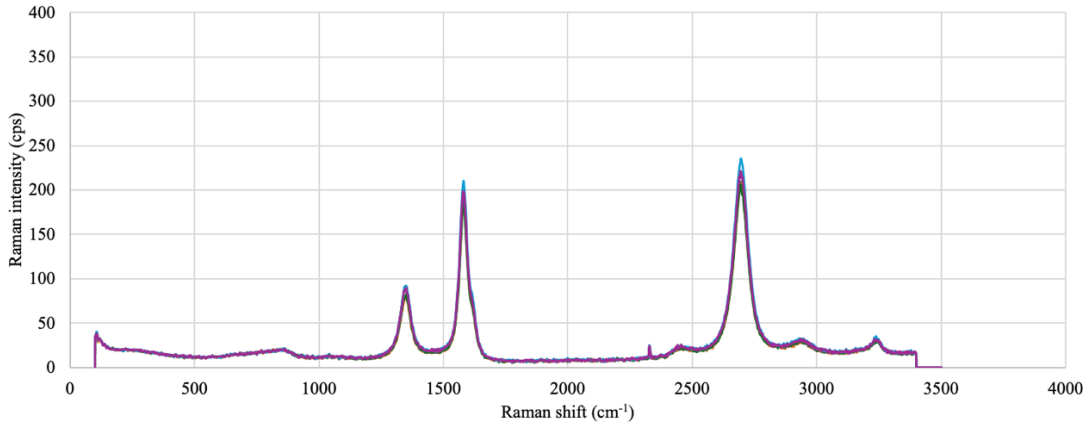

Figure 28: Raman spectra of 25 µm MWCNT filters

5.1.3. NH_2-MWCNT filters

5.1.3.1. Scanning electron microscopy

Figure 29 (a'), (b') and (c') show the NH_2-MWCNT coated SS mesh with grid opening sizes of 5, 10 and 25 µm, respectively. After NH_3 plasma treatment, there was no visible damage in the MWCNT network, agglomeration nor surface contamination.

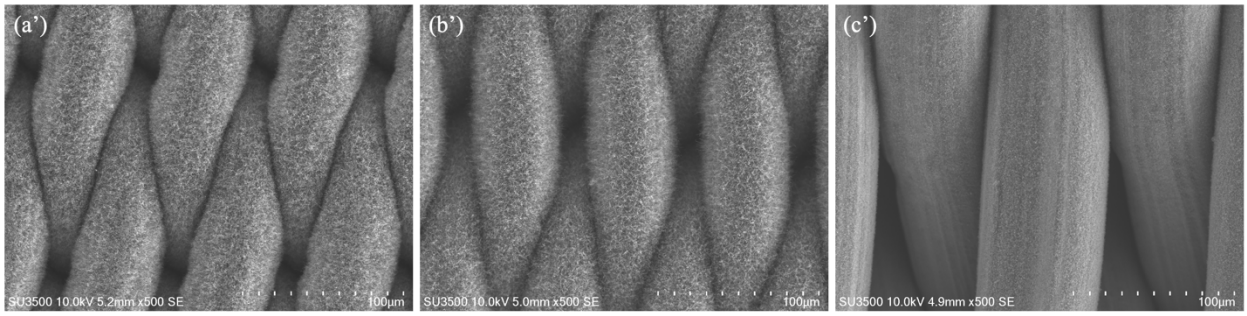

Figure 29: SEM images of NH_2-MWCNT filters (a') 5 µm (b') 10 µm (c') 25 µm

Figure 30, Figure 31, and Figure 32 display SEM images of the 5, 10 and 25 µm NH_2-MWCNT filters with ranging magnifications, respectively.

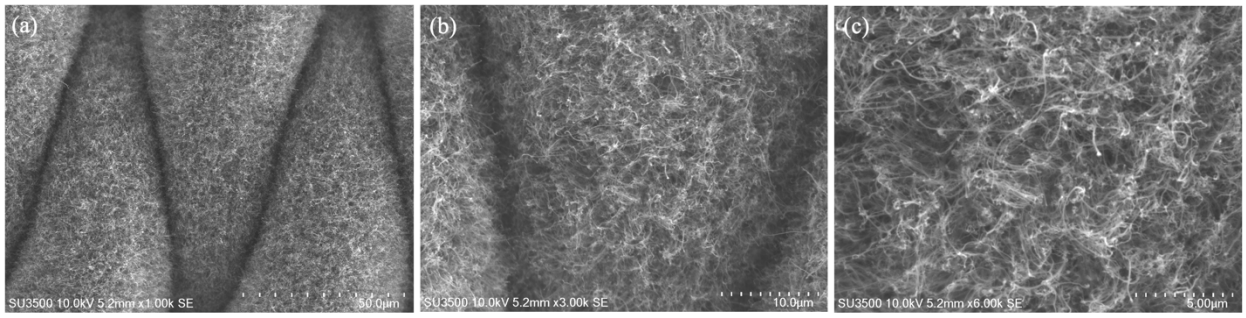

Figure 30: SEM images of 5 µm NH_2-MWCNT filters at different magnifications (a) ×1000 (b) ×3000 (c) ×6000

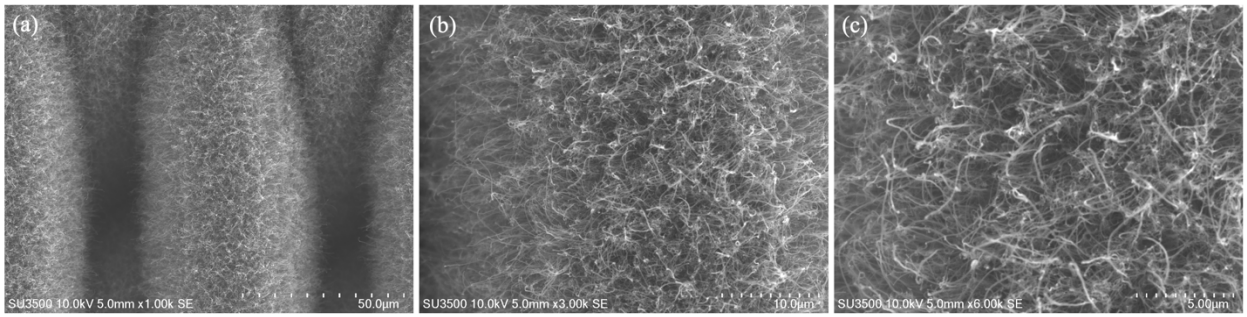

Figure 31: SEM images of 10 µm NH_2-MWCNT filters at different magnifications (a) ×1000 (b) ×3000 (c) ×6000

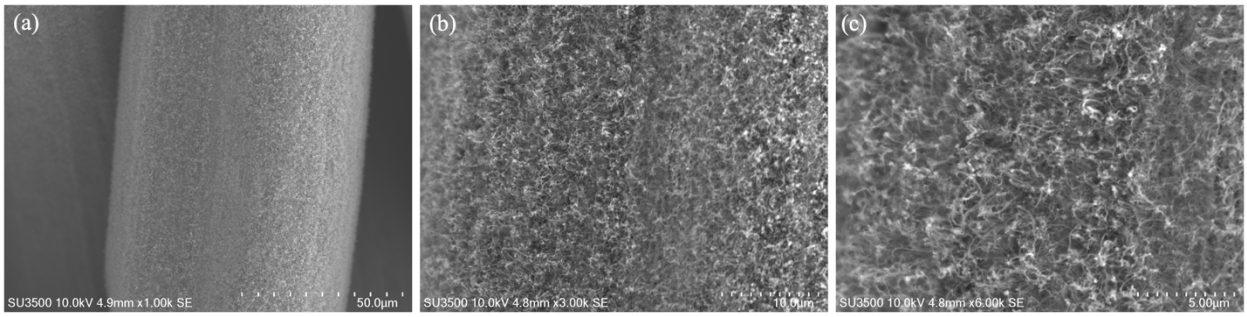

Figure 32: SEM images of 25 µm NH_2-MWCNT filters at different magnifications (a) ×1000 (b) ×3000 (c) ×6000

5.1.3.3. Water contact angle

Figure 33 (a'-c') displays the WCAs of the NH_2-MWCNT filters with varying pore sizes. After NH_3 plasma treatment, the surface properties of the hydrophobic MWCNT filters became completely hydrophilic having no detectable WCA.

Figure 33: WCAs of MWCNT and NH_2-MWCNT filters (a-a') 5 µm (b-b') 10 µm (c-c') 25 µm

5.1.3.4. Raman spectroscopy

The Raman spectra for the 5, 10 and 25 µm NH_2-MWCNT filters are displayed by Figure 34, Figure 35 and Figure 36, respectively.

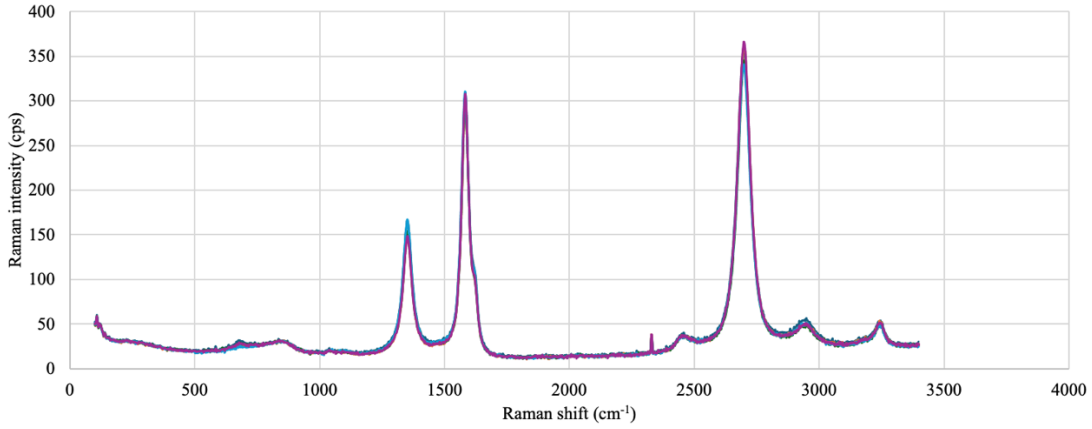

Figure 34: Raman spectra of 5 µm NH_2-MWCNT filters

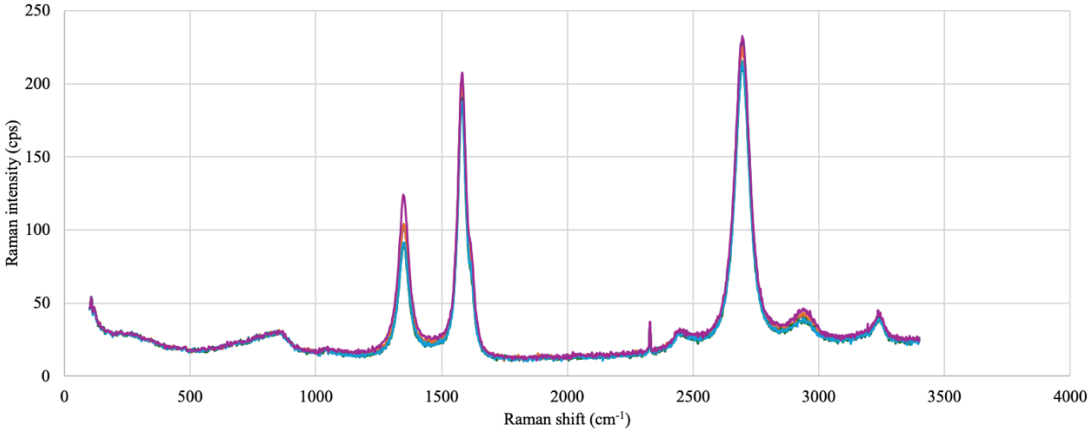

Figure 35: Raman spectra of 10 µm NH_2-MWCNT filters

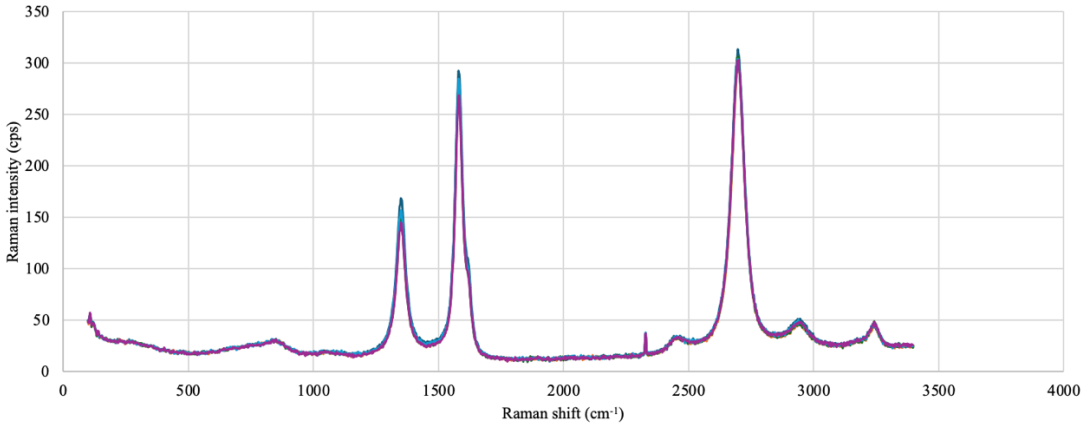

Figure 36: Raman spectra of 25 µm NH_2-MWCNT filters

Figure 37 displays the I_D/I_G ratios of the MWCNT and NH_2-MWCNT filters of varying pore sizes. The MWCNT filters had lower I_D/I_G ratios than the NH_2-MWCNT filters. The I_D/I_G for the 5,10 and 25 µm MWCNT filters were 0.43, 0.46, and 0.45, respectively. The lower I_D/I_G ratios confirm the pristine nature of the MWCNTs. After NH_3 functionalization, the 5, 10 and 25 µm filters had I_D/I_G ratios of 0.51, 0.52, and 0.55, respectively. The higher I_D/I_G ratios suggest a higher degree of disorder and defect in the MWCNT structure resulting from the NH_2 functional groups being grafted onto the surface and creating sp^3-hybridized carbon sites.

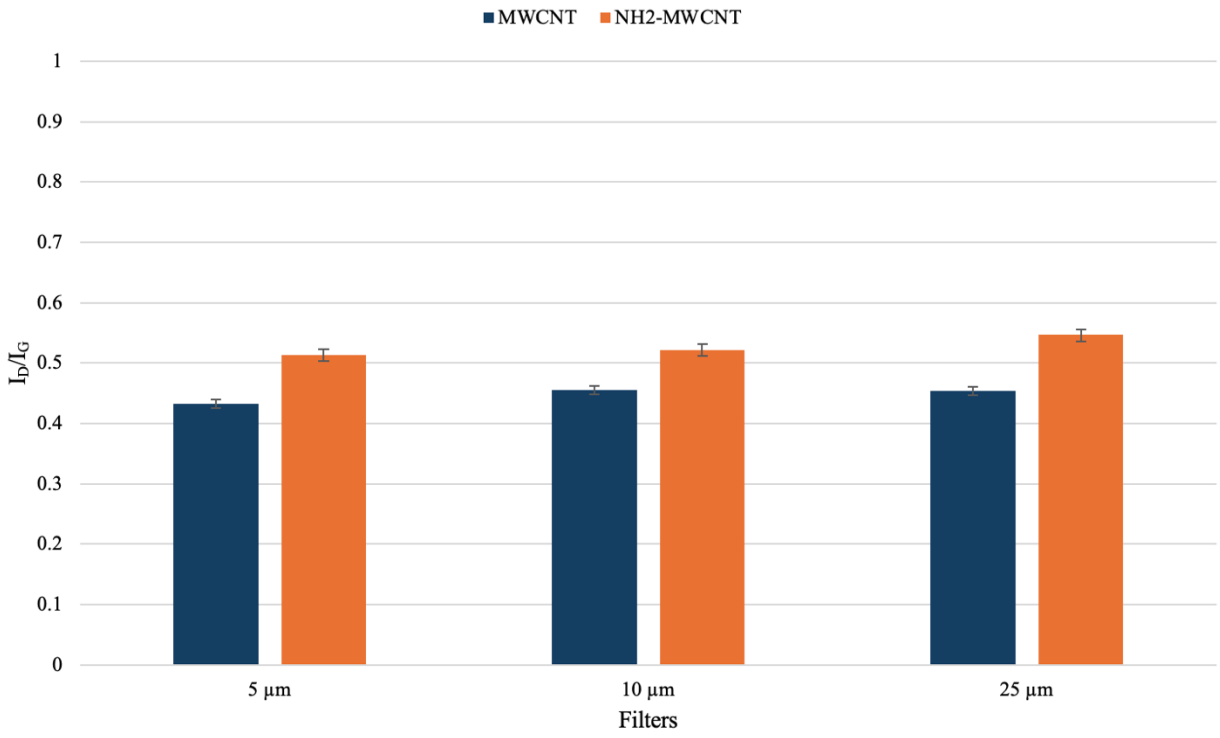

Figure 37: Bar graph displaying the I_D/I_G ratios of MWCNT and NH_2-MWCNT filters of varying pore sizes. Error bars represent the standard error (SE) (n=3).

5.2. Lymphocyte interaction

5.2.1. Spleen cell viability

5.2.1.1. MWCNT filters

The images captured using fluorescence microscopy are shown by Figure 38 and Figure 39. There was no visible green fluorescent calcein under the GFP fluorescence channel for the positive control which indicated cell death. The results of the filtered suspension through the 5, 10 and 25 μm MWCNT filters indicated cell viability as the spleen cells were fluorescing green under the GFP fluorescence channel.

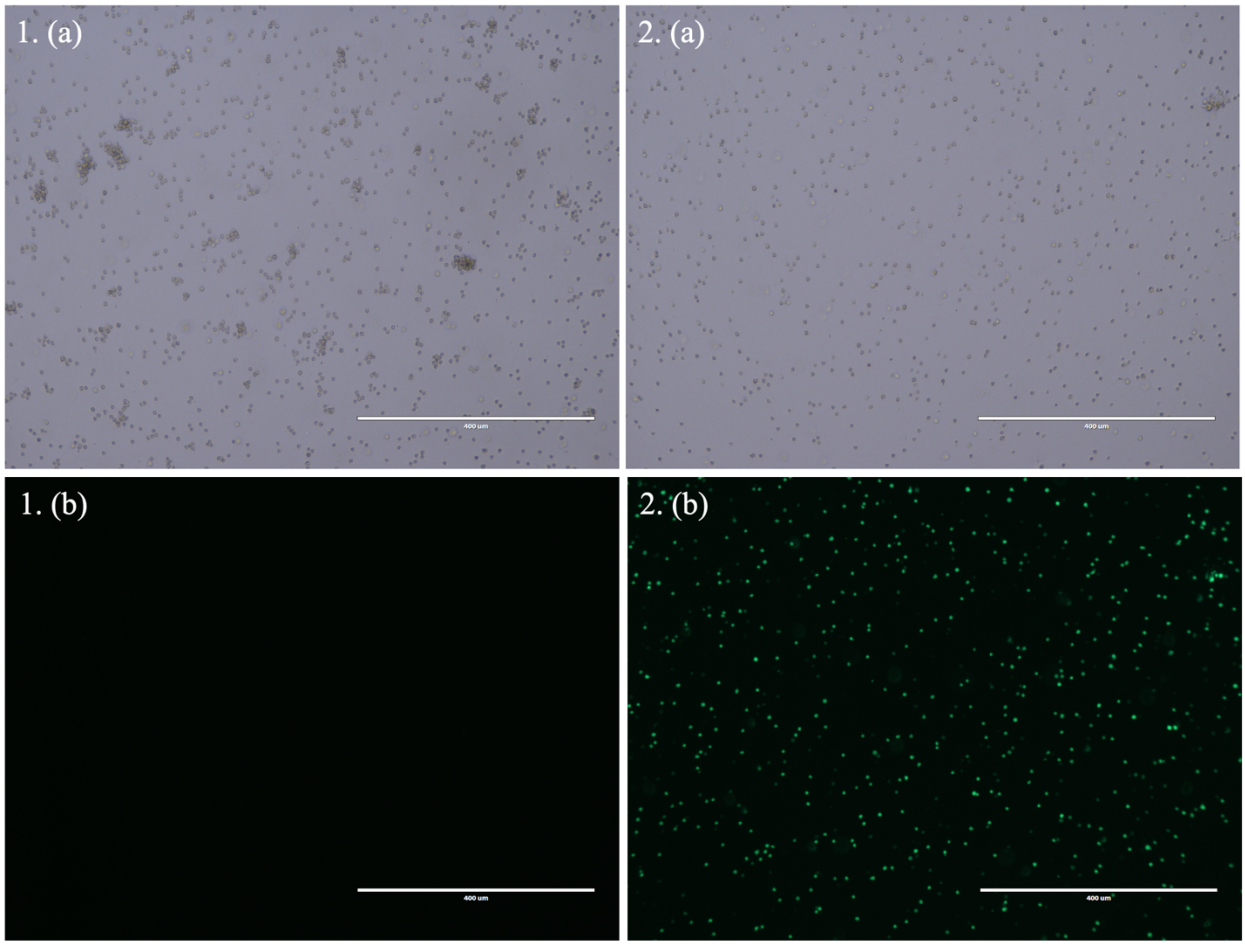

Figure 38: EVOS fluorescence microscopy images (a) TL (b) GFP 1. Positive control displaying cell death by heating suspension at 90 ˚C for 10 min 2. Filtered suspension through 5 µm MWCNT filter

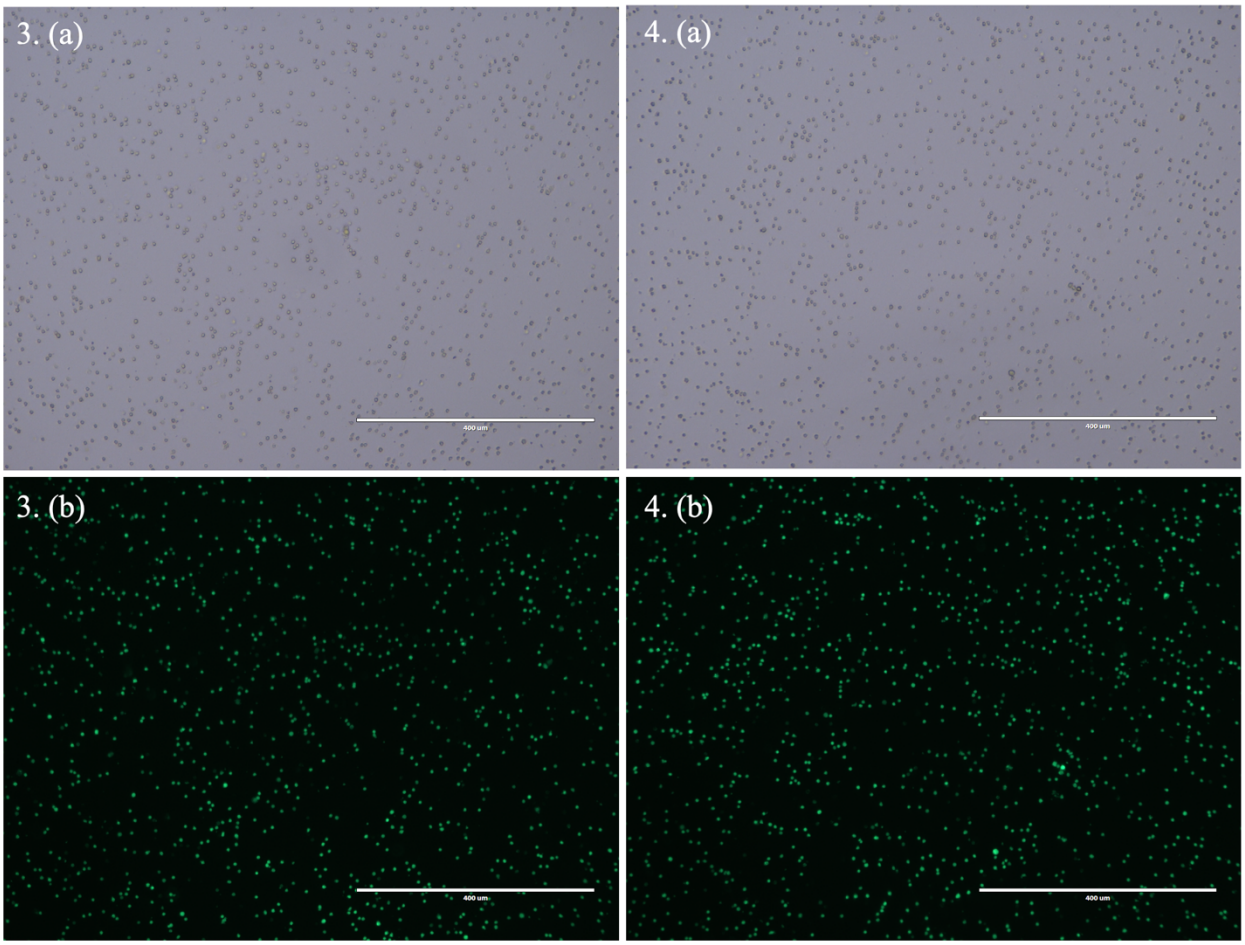

Figure 39: EVOS fluorescence microscopy images of filtered suspensions through 3. 10 µm and 4. 25 µm MWCNT filters (a) TL (b) GFP

Figure 40 displays a bar graph with information relating to the detected cells filtered through the MWCNT filters varying in pore size. The splenocytes passed through the filters as 34 %, 46 % and 45 % were viable through the 5, 10 and 25 µm MWCNT filters, respectively.

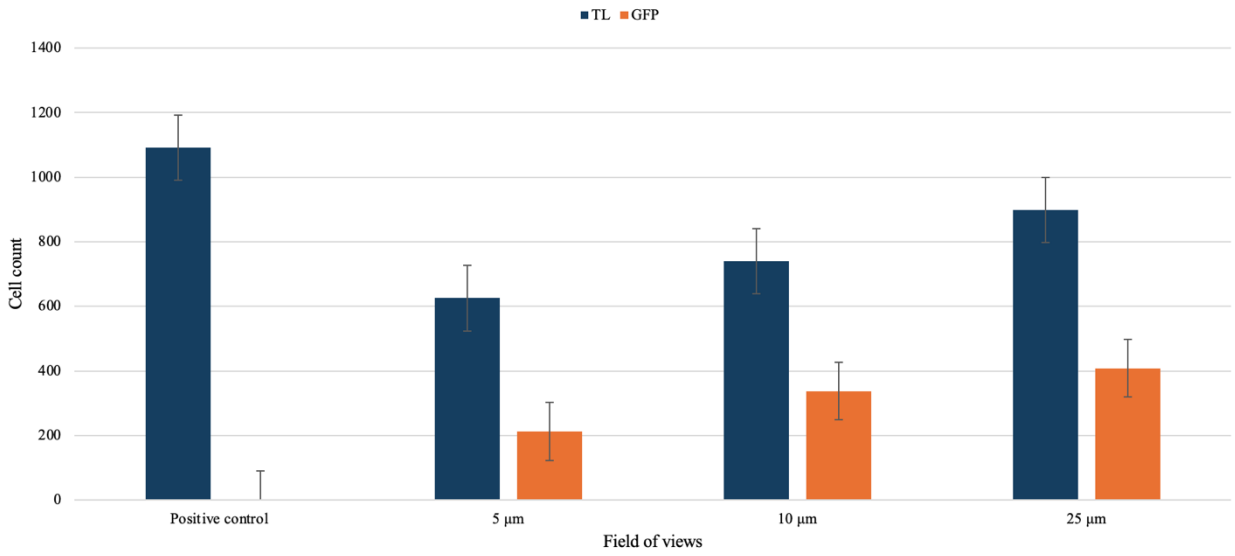

Figure 40: Bar graph showing the quantity of cells and viable cells that passed through MWCNT filters per FOV. Error bars indicate ± SE (n=3).

A probability (p)-value of 0.44 was calculated for the three independent splenocyte experimental groups for the proportion of viable cells over total cells through the MWCNT filters of various grid opening sizes. As the p-values were greater than the pre-emptively established 0.05 threshold, there was no statistically significant effect on the viability of splenocytes by passing them through MWCNT filters.

5.2.1.2. NH_2-MWCNT filters

The EVOS fluorescence microscopy images are shown by Figure 41 and Figure 42. The results of the filtered suspension through the 5, 10 and 25 µm NH_2-MWCNT filters indicated cell viability as the spleen cells were fluorescing green under the GFP fluorescence channel.

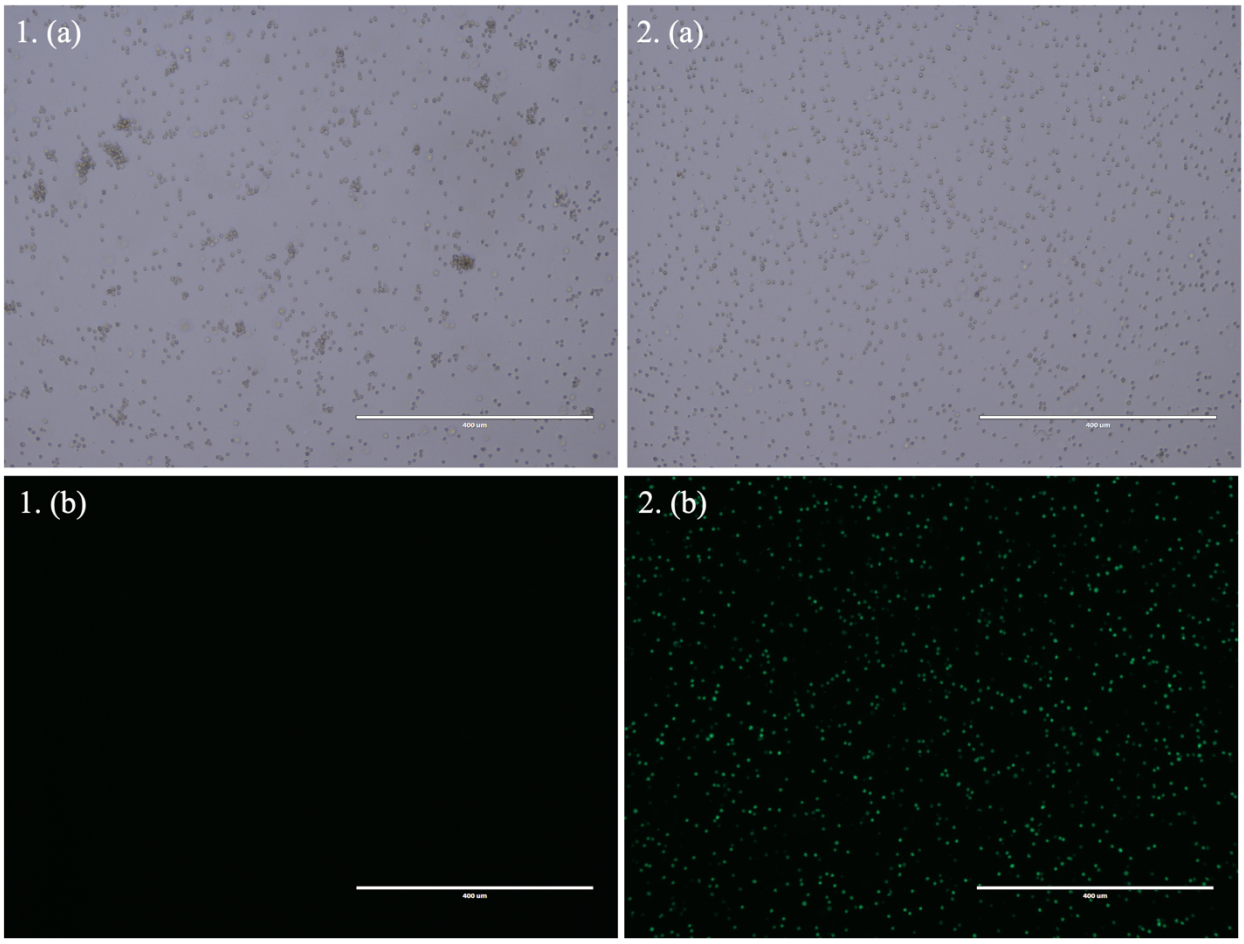

Figure 41: EVOS fluorescence microscopy images (a) TL (b) GFP 1. Positive control displaying cell death by heating suspension at 90 ˚C for 10 min 2. Filtered suspension through 5 µm NH_2-MWCNT filter

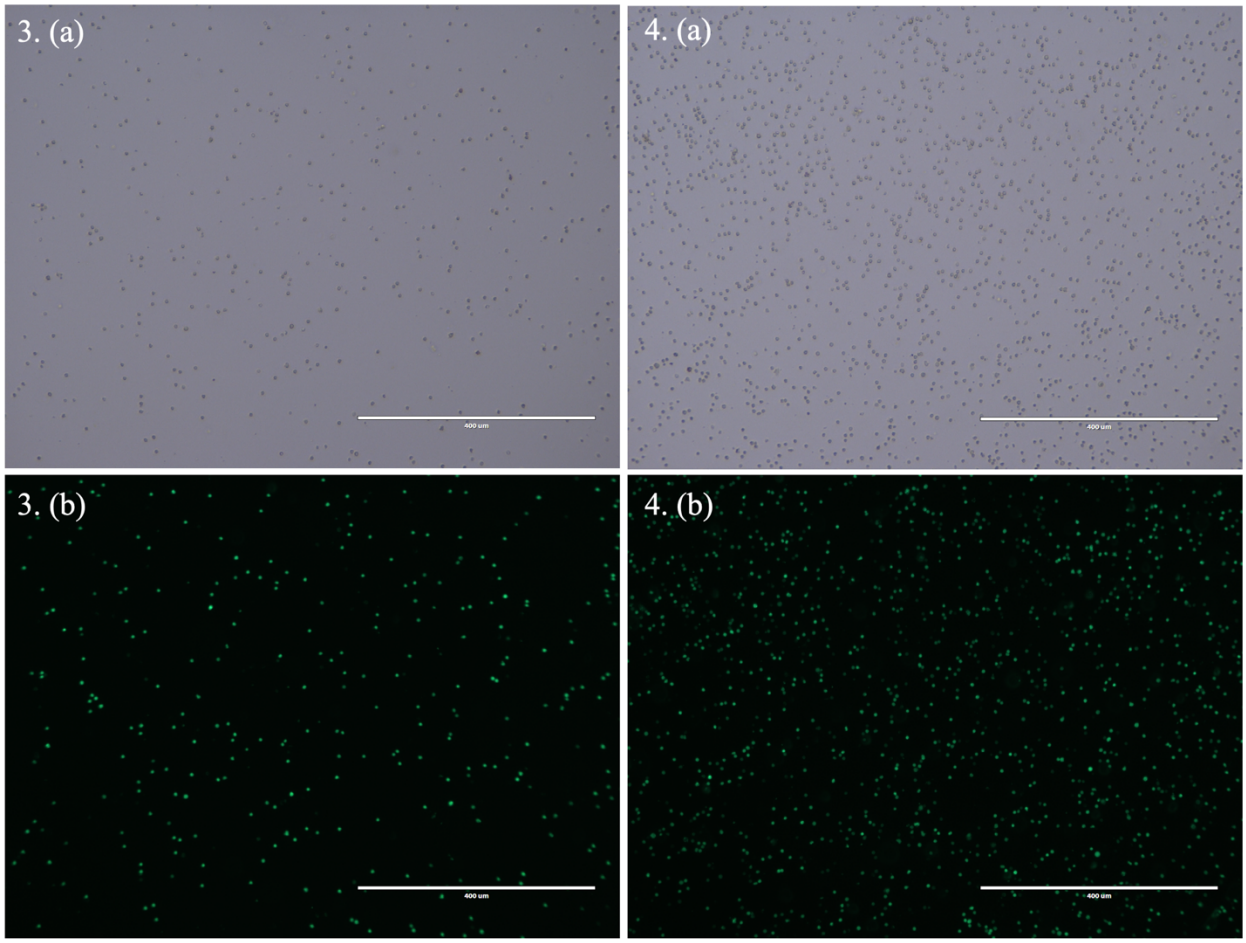

Figure 42: EVOS fluorescence microscopy images of filtered suspensions through 3. 10 µm and 4. 25 µm NH_2-MWCNT filter (a) TL (b) GFP

Figure 43 displays a bar graph with information relating to the detected cells filtered through the NH_2-MWCNT filters varying in pore size. 45 %, 36 % and 42 % of the splenocytes were viable after passing through the 5, 10 and 25 µm NH_2-MWCNT filters, respectively.

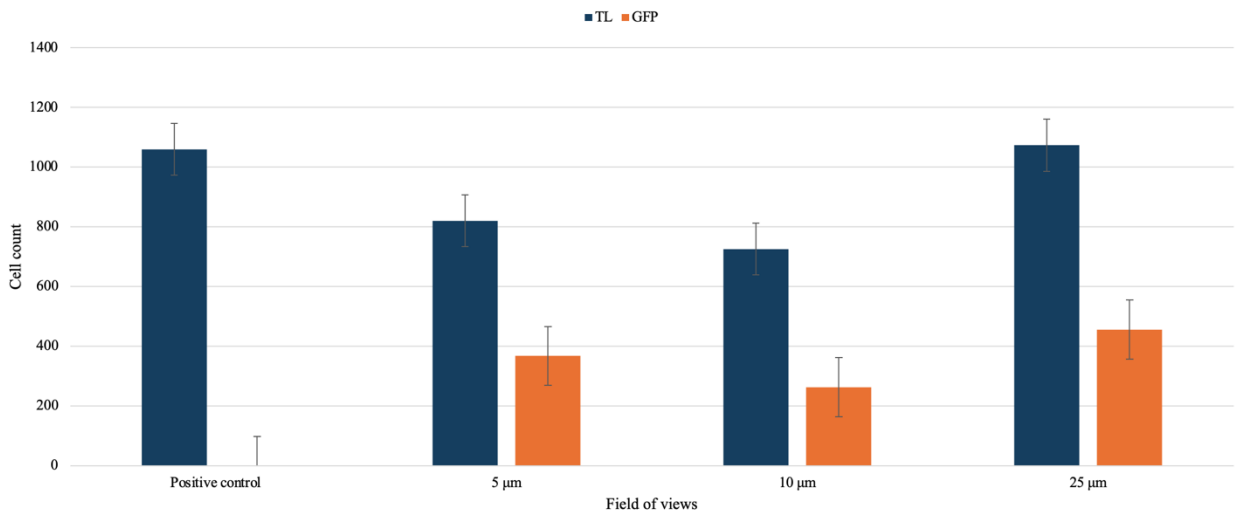

Figure 43: Bar graph showing the quantity of cells and viable cells that passed through NH_2-MWCNT filters per FOV. Error bars indicate ± SE (n=3).

A p-value of 0.16 for the three independent conditions of splenocyte through NH_2-MWCNT filters experiments was computed. The p-value was greater than 0.05 which suggested that the there was no statistically significant difference in splenocyte viability between the conditions or that the interaction of the splenocytes with the NH_2-MWCNT filters did not influence the viability of the cells.

Spleen cells are malleable which allowed them to conform to the 5 and 10 µm MWCNT and NH_2-MWCNT filters despite the larger diameter. The 25 µm MWCNT and NH_2-MWCNT filters performed similarly upon interaction with the splenocyte suspension. The larger pore size allowed more spleen cells to pass through the filter with less interference as there were minimal filter-cell interactions. An optimally performing filter would highly engage with the filter and provoke the least amount of cell death. Figure 44 is a comparison figure of cell viabilities after passing through the MWCNT and NH_2-MWCNT filters for the various pore sizes.

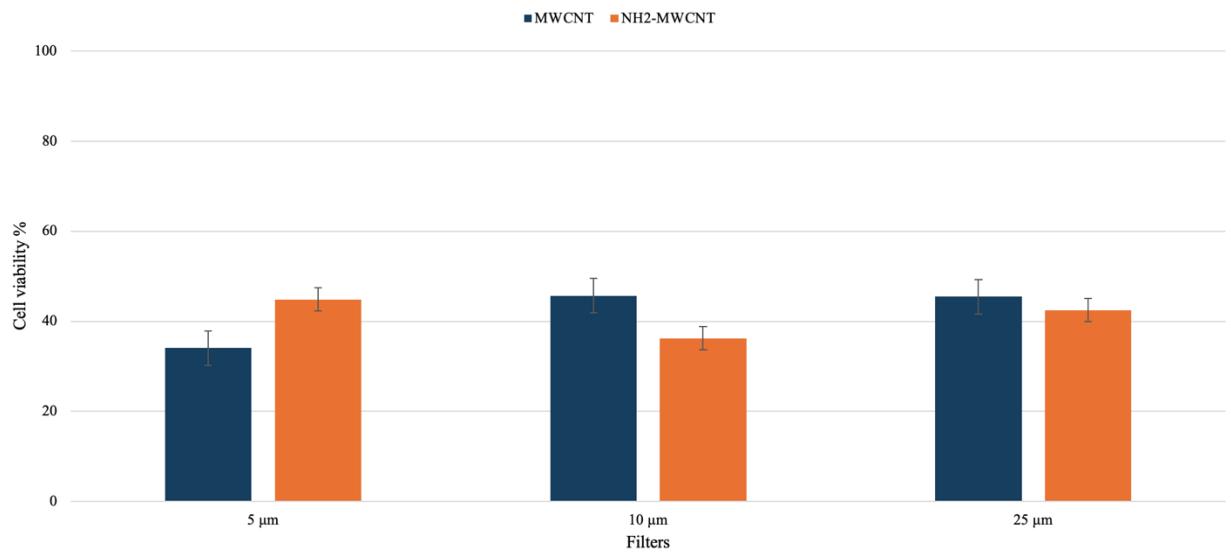

Figure 44: Comparison of cell viabilities between MWCNT and NH_2-MWCNT filters of varying pore sizes. Error bars indicate ± SE (n=3).

The MWCNT filters responded better to the splenocyte suspension than the NH_2-MWCNT filters. The 10 and 25 µm MWCNT filters led to slightly higher cell viability percentages despite being hydrophobic. The resistance between the hydrophobic surface and the splenocyte suspension did not damage the cells.

Limitations of the spleen cell viability experiment include not standardizing the dispensing speed which affected the forces being applied onto the MWCNT and NH_2-MWCNT filters. Therefore, this influenced how the splenocytes interacted with the MWCNT and NH_2-MWCNT filters. Furthermore, there was a delay in time from fabricating the filters to performing the biological testing due to the geographical distance separating the two laboratories where these experiments were carried out. The time lag can affect the functionality of the filters due to their exposure to the environment. Testing needs to be performed on the stability of the MWCNT and NH_2-MWCNT filters ensuring that their properties remain sound until the point of biological contact. Overall, the

experimental design of the spleen cell viability experiment needs to be modified to improve its statistical significance.

5.2.2. ELISA

Figure 45 is the standard curve generated for the ELISA assay. A linear trendline was used to model the data with a coefficient of determination of 0.99. The linear equation was used to determine the unknown concentrations of IFN-γ secreted in the splenocyte suspensions filtered through the MWCNT and NH_2-MWCNT filters.

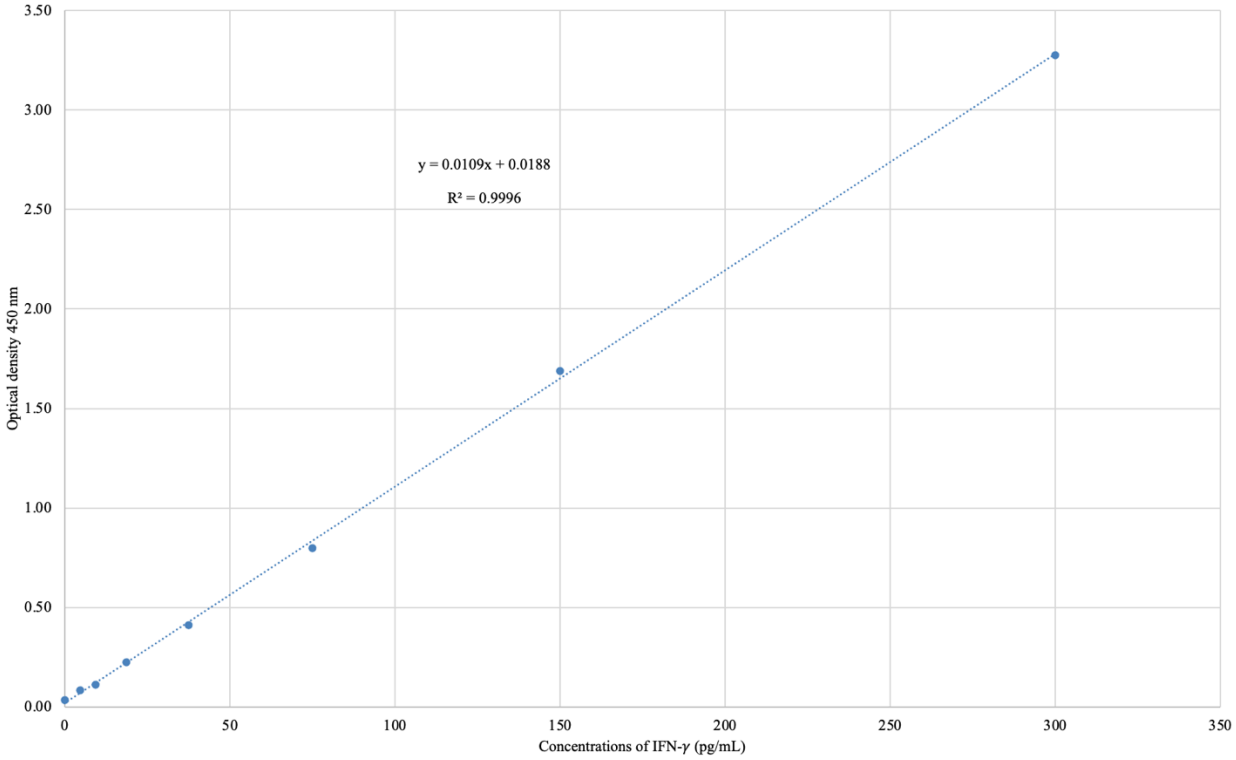

Figure 45: ELISA standard curve

The average of the detected concentrations of IFN-γ secreted in the duplicates of the various splenocyte suspensions are reported in Table 3.

Table 3: Measured concentrations of IFN-γ detected in splenocyte suspensions

Splenocyte suspensions	Pore size	Absorbances at 450 nm	Concentrations of IFN-γ (pg/mL)
PHA-L	-	4.85	443.35
Unfiltered splenocyte suspension	-	0.08	5.30
Heated suspension at 90˚C	-	0.05	2.95
MWCNT	5 µm	0.03	1.43
	10 µm	0.05	2.58
	25 µm	0.04	2.34
NH_2-MWCNT	5 µm	0.03	1.33
	10 µm	0.03	1.39
	25 µm	0.04	2.28

The optical density at 450 nm of the PHA-L sample was not within the range of the prepared standard solutions as it surpassed that of the higher limit of the IFN-γ standard of 300 pg/mL The extrapolated value for the concentration of IFN-γ for the PHA-L may be unreliable. For future ELISA experiments, the amount of PHA-L needs to be reduced to avoid the excessive cytokine production.

Low concentrations averaging 1.89 pg/mL of IFN-γ were reported in the filtered splenocyte suspensions through the MWCNT and NH_2-MWCNT filters of various pore sizes. Shear stresses alone were not sufficient in inducing the activation of T-cells. Therefore, this suggests that applied

normal forces should be incorporated with other methods to obtain the desired outcome of selective enhancement and proliferation of T-cells.

The NH_2-MWCNT filters will act as the foundational material for the immobilization of non-physiological agonists. Hypothesis 4 being the Ag-independent activation was not studied experimentally within the scope of this project. Before exploring Hypothesis 4, the amount of NH_2 functional groups on the surface of the NH_2-MWCNT filters needs to be quantified as to maximize the binding opportunities of the non-physiological agonists. After NH_3 plasma functionalization, a variety of nitrogen species were added to the MWCNT surfaces. Estimating the number of amine-functional groups using XPS is difficult as the XPS spectra cannot accurately distinguish the different types of nitrogen-containing functional groups [12]. Therefore, chemical derivatization can be performed as it is a technique that modifies the structure of a target compound to obtain an intermediate product with optimized chemical and physical properties compatible for XPS analysis [54].

Chapter 6

6. Conclusion

The aim of this project was to develop a functional nanomaterial filter that selectively detains immunosuppressive T-cells and induces the activation of T_{eff} cells by mechanical forces and non-physiological agonists. The filter material was composed of a dense network of high-purity and hydrophobic MWCNTs synthesized on 316L SS mesh. The MWCNT filters became hydrophilic with the addition of NH_2 groups after NH_3 plasma functionalization. A suspension of splenocytes was normally dispensed through the MWCNT and NH_2-MWCNT filters. The splenocyte viability experiments were not statistically significant when investigating the viability within splenocytes that passed through the MWCNT and NH_2-MWCNT filters. Low quantities of IFN-γ were secreted by the splenocytes after being dispensed normally through the MWCNT and NH_2-MWCNT filters. Mechanical forces alone did not induce the activation of T-cells while passing through the filters. The NH_2-MWCNT filters will act as the foundational material for future studies including the immobilization of non-physiological agonists. The combination of mechanically dispensing T-cells through NH_2-MWCNT filters coated with immobilized target antibodies was not explored in this project but may lead to the selective enhancement and proliferation of T-cells.

The future of this work includes addressing the shortcomings of this project. Potential improvements include:

i. Standardizing the dispensing flowrate of the splenocyte suspension using a syringe pump;
ii. Stabilizing the NH_2-MWCNT filters before biological testing;
iii. Quantifying the NH_2 groups on the surface of NH_2-MWCNT to maximize the immobilization potential of non-physiological agonists.

Chapter 7

7. References

[1] D. R. Brenner *et al.*, "Projected estimates of cancer in Canada in 2024," *CMAJ,* vol. 196, no. 18, pp. 615-623, May 2024, doi: 10.1503/cmaj.240095.

[2] S. K. Kim and S. W. Cho, "The Evasion Mechanisms of Cancer Immunity and Drug Intervention in the Tumor Microenvironment," *Front. Pharmacol.,* vol. 13, pp. 1-11, May 2022, doi: 10.3389/fphar.2022.868695.

[3] S. A. Rosenberg and N. P. Restifo, "Adoptive cell transfer as personalized immunotherapy for human cancer," *Science,* vol. 348, no. 6230, pp. 62-68, Apr. 2015, doi: 10.1126/science.aaa4967.

[4] R. A. Seder and R. Ahmed, "Similarities and differences in $CD4^+$ and $CD8^+$ effector and memory T cell generation," *Nat. Immunol.,* vol. 4, no. 9, pp. 835-842, Sep. 2003, doi: 10.1038/ni969.

[5] D. A. A. Vignali, L. W. Collison, and C. J. Workman, "How regulatory T cells work," *Nat. Rev. Immunol.,* vol. 8, no. 7, pp. 523-532, Jul. 2008, doi: 10.1038/nri2343.

[6] V. R. Raphey, T. K. Henna, K. P. Nivitha, P. Mufeedha, C. Sabu, and K. Pramod, "Advanced biomedical applications of carbon nanotube," *Mater. Sci. Eng. C Mater. Biol. Appl.,* vol. 100, pp. 616-630, Jul. 2019, doi: 10.1016/j.msec.2019.03.043.

[7] F. Choudhary, P. Mudgal, A. Parvez, P. Sharma, and H. Farooqi, "A review on synthesis, properties and prospective applications of carbon nanomaterials," *Nano-Struct. Nano-Objects.,* vol. 38, May 2024, Art. no. 101186, doi: 10.1016/j.nanoso.2024.101186.

[8] B. Murjani, P. Kadu, M. Bansod, S. Vaidya, and M. Yadav, "Carbon nanotubes in biomedical applications: current status, promises, and challenges," *Carbon Lett.,* vol. 32, pp. 1207-1226, Jul. 2022, doi: 10.1007/s42823-022-00364-4.

[9] Y. M. Manawi, A. Samara, T. Al-Ansari, and M. A. Atieh, "A Review of Carbon Nanomaterials' Synthesis via the Chemical Vapor Deposition (CVD) Method," *Mater.,* vol. 11, no. 5, May 2018, doi: 10.3390/ma11050822.

[10] W. Xiao-Di, K. Vinodgopal, and D. Gui-Ping, "Synthesis of Carbon Nanotubes by Catalytic Chemical Vapor Deposition," in *Perspect. of Carbon Nanotubes*, H. E.-D. Saleh and S. M. M. El Sheikh, Eds., London, U.K.: IntechOpen, 2019, pp.13-26.

[11] A. V. Okotrub *et al.*, "Distribution of Iron Nanoparticles in Arrays of Vertically Aligned Carbon Nanotubes Grown by Chemical Vapor Deposition," *Mater.,* vol. 15, no. 19, Sep. 2022, doi: 10.3390/ma15196639.

[12] C. Chen, B. Liang, D. Lu, A. Ogino, X. Wang, and M. Nagatsu, "Amino group introduction onto multiwall carbon nanotubes by NH_3/Ar plasma treatment," *Carbon,* vol. 48, no. 4, pp. 939-948, Apr. 2010, doi: 10.1016/j.carbon.2009.10.033.

[13] J. Lee *et al.*, "Ammonia-based plasma treatment of single-walled carbon nanotube thin films for bio-immobilization," *Carbon,* vol. 105, Apr. 2016, doi: 10.1016/j.carbon.2016.04.061.

[14] L. E. Vine and J. M. Schomaker, "Back to basics," *Nat. Chem.,* vol. 14, no. 10, pp. 1093-1094, Aug. 2022, doi: 10.1038/s41557-022-01029-5.

[15] J. Hancock, F. Rivera, B. Jensen, and R. Vanfleet, "Mechanisms for Chemical Vapor Deposition Carbon Nanotube Growth by Surface Modification of 316L Stainless Steel," *Microsc. Microanal.,* vol. 29, pp. 759-761, Jul. 2023, doi: 10.1093/micmic/ozad067.375.

[16] S. Bose, S. F. Robertson, and A. Bandyopadhyay, "Surface modification of biomaterials and biomedical devices using additive manufacturing," *Acta. Biomater.,* vol. 66, pp. 6-22, Jan. 2018, doi: 10.1016/j.actbio.2017.11.003.

[17] M. Zhianmanesh, A. Gilmour, M. M. M. Bilek, and B. Akhavan, "Plasma surface functionalization: A comprehensive review of advances in the quest for bioinstructive materials and interfaces," *Appl. Phys. Rev.,* vol. 10, no. 2, Apr. 2023, doi: 10.1063/5.0130829.

[18] E. Pajootan, M. Ye, M. Zhang, S. Niroumandrad, S. Omanovic, and S. Coulombe, "Plasma-functionalized multi-walled carbon nanotubes directly grown on stainless steel meshes as supercapacitor electrodes," *J. Phys. D: Appl. Phys.,* vol. 55, Feb. 2022, Art. no. 194001, doi: 10.1088/1361-6463/ac4fd8.

[19] L. Martinu, O. Zabeida, and J. E. Klemberg-Sapieha, "Chapter 9 - Plasma-Enhanced Chemical Vapor Deposition of Functional Coatings," in *Handbook of Deposition Technologies for Films and Coatings,* P. M. Martin, Ed., 3rd ed. Norwich, NY, USA: William Andrew Publishing, 2010, pp. 392-465.

[20] B. Alberts, A. Johnson, J. Lewis, M. Raff, K. Roberts, and P. Walter, *Molecular Biology of the Cell*, 4th ed. New York, NY, USA: Garland Science, 2002.

[21] K. E. O'Connell *et al.*, "Practical murine hematopathology: a comparative review and implications for research," *Comp. Med.,* vol. 65, no. 2, pp. 96-113, 2015.

[22] A. Tigner, S. A. Ibrahim, and I. V. Murray, *Histology, White Blood Cell*. Treasure Island, FL, USA: StatPearls Publishing, 2022.

[23] R. L. E. Cano, Eds. *Autoimmunity: From Bench to Bedside*. Bogota, Colombia: El Rosario University Press, 2013.

[24] L. Sun, Y. Su, A. Jiao, X. Wang, and B. Zhang, "T cells in health and disease," *Sig. Transduct. Target. Ther.,* vol. 8, pp. 235, Jun. 2023, Art. no. 235, doi: 10.1038/s41392-023-01471-y.

[25] H. Ahmed *et al.*, "Role of T cells in cancer immunotherapy: Opportunities and challenges," *Cancer Pathog. Ther.,* vol. 1, no. 2, pp. 116-126, Apr. 2023, doi: 10.1016/j.cpt.2022.12.002.

[26] D. Male, *Immunology: An Illustrated Outline*, 6th ed. Boca Raton, FL, USA: CRC Press, 2021, p. 175.

[27] K. Shah, A. Al-Haidari, J. Sun, and J. U. Kazi, "T cell receptor (TCR) signaling in health and disease," *Sig. Transduct. Target. Ther.,* vol. 6, pp. 412, Feb. 2021, Art. no. 412, doi: 10.1038/s41392-021-00823-w.

[28] F. Castro, A. P. Cardoso, R. M. Gonçalves, K. Serre, and M. J. Oliveira, "Interferon-Gamma at the Crossroads of Tumor Immune Surveillance or Evasion," *Front. Immunol.,* vol. 9, May 2018, doi: 10.3389/fimmu.2018.00847.

[29] T. Chinen *et al.*, "An essential role for the IL-2 receptor in T_{reg} cell function," *Nat. Immunol.,* vol. 17, no. 11, pp. 1322-1333, Sep. 2016, doi: 10.1038/ni.3540.

[30] B. Malik and A. Ghatol, "Understanding How Monoclonal Antibodies Work," in *StatPearls*. Treasure Island, FL, USA: StatPearls Publishing, 2024.

[31] L. L. Lu, T. J. Suscovich, S. M. Fortune, and G. Alter, "Beyond binding: antibody effector functions in infectious diseases," *Nat. Rev. Immunul.,* vol. 18, pp. 46-61, Oct. 2018, doi: 10.1038/nri.2017.106.

[32] C. Kuhn and H. L. Weiner, "Therapeutic Anti-Cd3 Monoclonal Antibodies: From Bench to Bedside," *Immunotherapy,* vol. 8, pp. 889-906, May 2016, doi: 10.2217/imt-2016-0049.

[33] Y. Choi, Y. Shi, C. L. Haymaker, A. Naing, G. Ciliberto, and J. Hajjar, "T-cell agonists in cancer immunotherapy," *J. Immunother. Cancer,* vol. 8, no. 2, Oct. 2020, doi: 10.1136/jitc-2020-000966.

[34] B. J. Chen, J. W. Zhao, D. H. Zhang, A. H. Zheng, and G. Q. Wu, "Immunotherapy of Cancer by Targeting Regulatory T cells," *Int. Immunopharmacol.,* vol. 104, Mar. 2022, Art. no. 108469, doi: 10.1016/j.intimp.2021.108469.

[35] D. L. Harrison, Y. Fang, and J. Huang, "T-Cell Mechanobiology: Force Sensation, Potentiation, and Translation," *Front. Phys.,* vol. 7, Apr. 2019, doi: 10.3389/fphy.2019.00045.

[36] N. Jeffreys, J. Brockman, Y. Zhai, D. Ingber, and D. Mooney, "Mechanical forces amplify TCR mechanotransduction in T cell activation and function," *Appl. Phys. Rev.,* vol. 11, Mar. 2024, doi: 10.1063/5.0166848.

[37] G. Constantin and C. Laudanna, "Transmigration of effector T lymphocytes: changing the rules," *Nat. Immunol.,* vol. 13, pp. 15-16, Jan. 2012, doi: 10.1038/ni.2188.

[38] M. Aramesh, D. Stoycheva, L. Raaz, and E. Klotzsch, "Engineering T-cell activation for immunotherapy by mechanical forces," *Curr. Opin. Biomed. Eng.,* vol. 10, pp. 134-141, Jun. 2019, doi: 10.1016/j.cobme.2019.05.004.

[39] M. Fritzsche and K. Kruse, "Mechanical force matters in early T cell activation," *Proc. Natl. Acad. Sci.,* vol. 121, no. 37, Jun. 2024, Art. no. e2404748121, doi: 10.1073/pnas.2404748121.

[40] D. Sun, X. Shi, S. Li, X. Wang, X. Yang, and M. Wan, "CAR-T cell therapy: A breakthrough in traditional cancer treatment strategies," *Mol. Med. Rep.,* vol. 29, no. 3, Mar. 2024, doi: 10.3892/mmr.2024.13171.

[41] Y. Liu *et al.*, "TCR-T Immunotherapy: The Challenges and Solutions," *Front. Oncol.,* vol. 11, Jan. 2022, doi: 10.3389/fonc.2021.794183.

[42] J. Haanen, C. Los, G. Q. Phan, and A. B. Warner, "Adoptive Cell Therapy for Solid Tumors: Current Status in Melanoma and Next-Generation Therapies," *Am. Soc. Clin. Oncol. Educ. Book,* vol. 44, May 2024, Art. no. e431608, doi: 10.1200/edbk_431608.

[43] M. W. Rohaan, S. Wilgenhof, and J. Haanen, "Adoptive cellular therapies: the current landscape," *Virchows Arch.,* vol. 474, no. 4, pp. 449-461, Apr. 2019, doi: 10.1007/s00428-018-2484-0.

[44] M. I. Sajid, U. Jamshaid, T. Jamshaid, N. Zafar, H. Fessi, and A. Elaissari, "Carbon nanotubes from synthesis to in vivo biomedical applications," *Int. J. Pharm.,* vol. 501, no. 1-2, pp. 278-99, Mar. 2016, doi: 10.1016/j.ijpharm.2016.01.064.

[45] Y. M. Manawi, Ihsanullah, A. Samara, T. Al-Ansari, and M. A. Atieh, "A Review of Carbon Nanomaterials' Synthesis via the Chemical Vapor Deposition (CVD) Method," *Materials,* vol. 11, no. 5, pp. 822, May 2018. [Online]. Available: https://www.mdpi.com/1996-1944/11/5/822.

[46] L. Camilli *et al.*, "The synthesis and characterization of carbon nanotubes grown by chemical vapor deposition using a stainless steel catalyst," *Carbon,* vol. 49, no. 10, pp. 3307-3315, Aug. 2011, doi: 10.1016/j.carbon.2011.04.014.

[47] J. Hancock, F. Rivera, B. Jensen, and R. Vanfleet, "Mechanisms for Chemical Vapor Deposition Carbon Nanotube Growth by Surface Modification of 316L Stainless Steel," *Microsc. Microanal.,* vol. 29, no. Supplement_1, pp. 759-761, Jul. 2023, doi: 10.1093/micmic/ozad067.375.

[48] N. Hordy, S. Coulombe, and J.-L. Meunier, "Plasma Functionalization of Carbon Nanotubes for the Synthesis of Stable Aqueous Nanofluids and Poly(vinyl alcohol) Nanocomposites," *Plasma Processes and Polymers,* vol. 10, no. 2, pp. 110-118, Sep. 2013, doi: 10.1002/ppap.201200075.

[49] L. Jorge, P.-L. Girard-Lauriault, and S. Coulombe, "pH-reversible destabilization-dispersion of MWCNTs coated with functional plasma polymer films in water," *Plasma Processes and Polymers,* vol. 14, Apr. 2017, Art. no. 1700026, doi: 10.1002/ppap.201700026.

[50] L. Hein, E. Friesen, G. D. Placido, and S. Coulombe, "Attachment of Amine Groups to Multi-Walled Carbon Nanotubes by Non-Thermal Radiofrequency Ammonia (NH_3), Argon (Ar) and Hydrogen (H_2) Plasma Functionalization," unpublished.

[51] "2018 Teklad Global 18% Protein Rodent Diets." Inotiv.com. Accessed: Sep. 15, 2024. [Online]. Available: https://www.inotiv.com/rodent-natural-ingredient-2018-diets

[52] L. Gutiérrez *et al.*, "1.09 - Nanotechnology in Drug Discovery and Development," in *Comprehensive Medicinal Chemistry III*, S. Chackalamannil, D. Rotella, and S. E. Ward Eds. Oxford, England: Elsevier, 2017, pp. 264-295.

[53] H. J. Butler *et al.*, "Using Raman spectroscopy to characterize biological materials," *Nat. Protoc.,* vol. 11, no. 4, pp. 664-687, Mar. 2016, doi: 10.1038/nprot.2016.036.

[54] J. Y. Yook, J. Jun, and S. Kwak, "Amino functionalization of carbon nanotube surfaces with NH_3 plasma treatment," *Appl. Surf. Sci.,* vol. 256, no. 23, pp. 6941-6944, Apr. 2010, doi: 10.1016/j.apsusc.2010.04.075.